Discover Oncology

Analysis

Development of a machine learning-based predictive risk model combining fatty acid metabolism and ferroptosis for immunotherapy response and prognosis in prostate cancer

Zhenwei Wang[1,2] · Zhihong Dai[1] · Yuren Gao[1] · Zhongxiang Zhao[2] · Zhen Li[1] · Liang Wang[1] · Xiang Gao[1] · Qiuqiu Qiu[4] · Xiaofu Qiu[2,3] · Zhiyu Liu[1]

Received: 11 February 2025 / Accepted: 24 April 2025
Published online: 13 May 2025

Abstract

Prostate cancer (PCa) remains a leading cause of cancer-related mortality, necessitating robust prognostic models and personalized therapeutic strategies. This study integrated bulk RNA sequencing, single-cell RNA sequencing (scRNA-seq), and spatial transcriptomics to construct a prognostic model based on genes shared between ferroptosis and fatty acid metabolism (FAM). Using the TCGA-PRAD dataset, we identified 73 differentially expressed genes (DEGs) at the intersection of ferroptosis and FAM, of which 19 were significantly associated with progression-free survival (PFS). A machine learning-based prognostic model, optimized using the Lasso + Random Survival Forest (RSF) algorithm, achieved a high C-index of 0.876 and demonstrated strong predictive accuracy (1-, 2-, and 3-year AUCs: 0.77, 0.75, and 0.78, respectively). The model, validated in the DFKZ cohort, stratified patients into high- and low-risk groups, with the high-risk group exhibiting worse PFS and higher tumor mutation burden (TMB). Functional enrichment analysis revealed distinct pathway activities, with high-risk patients showing enrichment in immune-related and proliferative pathways, while low-risk patients were enriched in metabolic pathways. Immune microenvironment analysis revealed heightened immune activity in high-risk patients, characterized by increased infiltration of CD8 + T cells, regulatory T cells, and M2 macrophages, alongside elevated TIDE scores, suggesting immune evasion and resistance to immunotherapy. In contrast, low-risk patients exhibited higher infiltration of plasma cells and neutrophils and demonstrated better responses to immune checkpoint inhibitors (ICIs). Spatial transcriptomics and scRNA-seq further elucidated the spatial distribution of model genes, highlighting the central role of macrophages in mediating risk stratification. Additionally, chemotherapy sensitivity analysis identified potential therapeutic agents, such as Erlotinib and Picolinic acid, for low-risk patients. In vitro experiments showed that overexpression of CD38 in the PC-3 cell line led to elevated lipid peroxidation (C11-BODIPY) and reactive oxygen species (ROS), suggesting increased cell ferroptosis. These findings provide a comprehensive framework for risk stratification and personalized treatment in PCa, bridging molecular mechanisms with clinical outcomes.

Zhenwei Wang, Zhihong Dai, Yuren Gao and Zhongxiang Zhao have contributed equally to this work and were considered co-first authors.

Supplementary Information The online version contains supplementary material available at https://doi.org/10.1007/s12672-025-02484-5.

✉ Qiuqiu Qiu, qiuqq1992@163.com; ✉ Xiaofu Qiu, qiuxf@gd2h.org.cn; ✉ Zhiyu Liu, lzydoct@163.com | [1]Department of Urology, Second Hospital of Dalian Medical University, Dalian 116023, China. [2]Department of Urology, The Affiliated Guangdong Second Provincial General Hospital of Jinan University, Guangzhou 510317, China. [3]The Second School of Clinical Medicine, Southern Medical University, Guangzhou 510317, China. [4]Department of Urology, Gaohou People's Hospital, Maoming 525200, China.

Keywords Prostate cancer · Machine learning · Tumor microenvironment · Fatty acid metabolism · Ferroptosis · Multi-omics

1 Introduction

Prostate cancer is one of the most common malignancies among men worldwide, with significant morbidity and mortality. In 2022, prostate cancer accounted for 7.3% of all newly diagnosed tumors, ranking as the fourth most common cancer globally. Additionally, the disease was responsible for 396,792 deaths, making it the eighth leading cause of cancer-related mortality [1]. Advances in research have enhanced our understanding of its molecular underpinnings, including the role of androgen receptor signaling and genetic mutations. However, challenges persist in early detection due to the heterogeneity of the disease and the limitations of screening tools. Treatment strategies, such as surgery, radiotherapy, and androgen deprivation therapy, face difficulties with resistance development and balancing efficacy with quality of life. Novel therapies are under exploration to improve outcomes.

Fatty acid metabolism plays a critical role in cellular energy homeostasis, membrane biosynthesis, and signaling, making it a vital process for both normal and cancerous cells [2, 3]. In tumors, including prostate cancer, dysregulated fatty acid metabolism supports rapid proliferation, survival under stress, metastasis, and effects of immunotherapy [4, 5]. Cancer cells often upregulate de novo lipogenesis through increased expression of enzymes like fatty acid synthase (FASN), stearoyl-CoA desaturase (SCD), and acetyl-CoA carboxylase (ACC) [6–8]. Concurrently, enhanced fatty acid uptake and beta-oxidation provide additional energy and biosynthetic precursors necessary for tumor growth [2]. In prostate cancer, androgen signaling heavily influences lipid metabolism, further promoting lipid accumulation and metabolic reprogramming [9]. This dependency on fatty acid metabolism is particularly evident in advanced, castration-resistant prostate cancer (CRPC), where alterations in lipid pathways correlate with aggressive behavior and therapeutic resistance [10]. Lipids also serve as signaling molecules, modulating pathways like PI3K/AKT/mTOR and inflammation, contributing to tumor progression [10]. The relevance of fatty acid metabolism to prostate cancer highlights its potential as a therapeutic target. Inhibitors of FASN, ACC, or fatty acid transport proteins are under investigation, aiming to disrupt the metabolic vulnerabilities of cancer cells. Understanding the interplay between fatty acid metabolism and tumor biology could pave the way for novel strategies to improve patient outcomes [11].

Ferroptosis is a regulated form of cell death characterized by iron-dependent lipid peroxidation and oxidative stress, distinct from apoptosis, necrosis, and autophagy. It occurs due to the imbalance between the production of reactive oxygen species (ROS) and the antioxidant defense system, primarily involving glutathione peroxidase 4 (GPX4), which detoxifies lipid peroxides [12]. In cancer, ferroptosis has garnered attention for its dual role: while cancer cells often develop mechanisms to evade ferroptosis, its induction represents a promising therapeutic strategy [12]. In prostate cancer, particularly in advanced and castration-resistant stages, ferroptosis is highly relevant. Prostate cancer cells frequently exhibit alterations in lipid metabolism and oxidative stress pathways, creating vulnerabilities to ferroptosis. For instance, heightened iron accumulation and dysregulated lipid metabolism in these cells increases susceptibility to ferroptotic triggers [13]. Moreover, therapeutic resistance, a major challenge in prostate cancer treatment, has been linked to ferroptosis evasion mechanisms such as the upregulation of GPX4 and the cystine/glutamate antiporter (system Xc −). Targeting ferroptosis pathways holds promise for overcoming resistance and selectively killing prostate cancer cells. Agents like GPX4 inhibitors or drugs that enhance lipid peroxidation are under investigation. Understanding the complex role of ferroptosis in tumor biology may unlock novel approaches to improve outcomes in prostate cancer.

Fatty acid metabolism critically regulates ferroptosis by determining membrane lipid composition. PUFAs (e.g., arachidonic acid) are highly prone to peroxidation due to their multiple double bonds. Acyl-CoA synthetase long-chain family member 4 (ACSL4) activates and incorporates PUFAs into phosphatidylethanolamine phospholipids, enhancing membrane susceptibility to oxidative damage [14, 15]. High ACSL4 expression correlates with ferroptosis sensitivity, while its suppression reduces PUFA levels and confers resistance. Conversely, monounsaturated fatty acids (MUFAs), such as oleic acid, antagonize ferroptosis by replacing PUFAs in membranes, lowering peroxidation risk. Stearoyl-CoA desaturase-1 (SCD1), which synthesizes MUFAs from saturated fatty acids, promotes this protective shift. Thus, the ACSL4/SCD1 axis balances PUFA-MUFA ratios, acting as a metabolic checkpoint for ferroptosis [16]. Fatty acid uptake and storage further modulate susceptibility. CD36, a fatty acid transporter, increases PUFA influx, exacerbating peroxidation [17]. Lipid droplets sequester free fatty acids, limiting PUFA availability for membrane incorporation; their dysfunction elevates free PUFA pools, amplifying ferroptosis. Enzymes like lipoxygenases (LOXs) directly oxidize PUFAs, driving peroxidation [18]. Systemic metabolic pathways, such as fatty acid oxidation (FAO), may indirectly influence ferroptosis by altering redox

states or energy supplies, though mechanisms remain unclear. Therapeutically, this interplay offers promise. Cancers with high ACSL4 or PUFA uptake may be targeted with ferroptosis inducers, while neurodegenerative diseases marked by lipid peroxidation (e.g., Alzheimer's) might benefit from MUFA-enhancing strategies. Targeting lipid metabolism enzymes (ACSL4, SCD1), transporters (CD36), or peroxidation pathways (LOXs) could fine-tune ferroptosis in disease contexts, underscoring its potential as a precision medicine tool. In this study, we aimed to investigate the relationship between fatty acid metabolism and ferroptosis in prostate cancer. To achieve this, we constructed a prognostic model using machine learning by identifying genes commonly associated with the prognosis of both processes. Through a series of multi-omics analyses, we identified a set of 12 shared genes in prostate cancer that are co-involved in fatty acid metabolism and iron death which provided mechanistic insights into its potential role in disease progression and therapeutic response.

2 Methods and materials

2.1 Acquisition and procession of public data

We obtained bulk RNA sequencing expression data and corresponding clinical information from the PRAD project in The Cancer Genome Atlas (TCGA) database (https://portal.gdc.cancer.gov/) and the DFKZ-PRAD project in the cBioPortal database (https://www.cbioportal.org/). The single-cell RNA sequencing data (GSE141445) were retrieved from the Gene Expression Omnibus (GEO, https://www.ncbi.nlm.nih.gov/geo/). Immunotherapy cohort data were downloaded using the "IMvigor210CoreBiologies" package. Additionally, a total of 2,399 fatty acid metabolism-related genes were compiled from the MSigDB database (https://www.gsea-msigdb.org/gsea/msigdb) and relevant literature [19, 20]. 780 Ferroptosis-related genes were sourced from the FerrDb V2 database (http://www.zhounan.org/ferrdb/current/).

2.2 Construction and evaluation of prognostic model via 113 combinations of machine learning algorithms

Differential expression analysis of tumor and adjacent tissue samples from the TCGA prostate cancer dataset was conducted using the "limma" R package, identifying differentially expressed genes (DEGs) with an adjusted $p < 0.05$ and $|\log2 \text{ fold change (FC)}| \geq 1$. The intersection of DEGs with fatty acid metabolism and ferroptosis-related genes was then analyzed for their association with progression-free survival (PFS) prognosis using univariate regression analysis, with a threshold of $p < 0.05$, to identify prognosis-related genes. The identified genes were then evaluated through 113 combinations of machine learning algorithms, including Partial Least Squares Regression (plsRcox), SuperPC, the least absolute shrinkage and selection operator (Lasso), ridge regression (Ridge), Gradient Boosting Machine (GBM), elastic net (Enet), stepwise Cox regression (StepCox), survival support vector machine (survivalSVM), Random Survival Forest (RSF), CoxBoost, and Linear Discriminant Analysis (LDA), using tenfold cross-validation to prevent overfitting and determine the optimal prognostic model in the training and testing cohorts. To evaluate the performance of the constructed model, its predictive ability was assessed using ROC curves generated by the "pROC" package. To determine whether the risk score could serve as an independent factor for PFS in PRAD, we performed univariate and multivariate Cox regression analyses. Kaplan–Meier (K-M) survival plots for the training and testing cohorts were analyzed using the "survminer" package. Additionally, a nomogram integrating clinical factors and risk scores was constructed using the "rms" package.

2.3 Annotation of functional pathways and tumor mutation burden (TMB) analysis

The DEGs between the two groups were identified using the "limma" method. Subsequently, the "org.Hs.eg.db" and "clusterProfiler" packages were applied to annotate the enriched gene ontology and Kyoto Encyclopedia of Genes and Genomes (KEGG) pathways associated with the DEGs. Additionally, somatic variation data from the TCGA-PRAD cohort were analyzed using the "maftools'" package to calculate the frequency of copy number variations (CNVs), as well as to identify the affected pathways and genes.

2.4 Immune cell infiltration and prediction of immunotherapy response

The ESTIMATE algorithm was used to calculate stromal, immune, and ESTIMATE scores, assessing immune cell infiltration differences between groups. CIBERSORT evaluated infiltration scores for 28 immune cell types. Spearman's correlation analyzed the relationship between immune infiltration and model gene expression. The risk score system was used to predict immunotherapy response. Data from the Tumor Immune Dysfunction and Exclusion (TIDE) (http://tide.dfci.harvard.edu) assessed clinical efficacy across risk groups, including TIDE, microsatellite instability (MSI), dysfunction, and exclusion scores. The IMvigor210 Cohort clinical trial evaluated atezolizumab (anti-PD-L1) in metastatic urothelial carcinoma. Risk scores were compared between patients with disease/stable disease (PD/SD) vs. complete response/partial response (CR/PR). The Chi-square test assessed PD/SD and CR/PR distributions across risk groups.

2.5 Sensitivity of chemotherapy and screening of potential drugs

The prediction of chemotherapy response was performed using the R package "pRRophetic," which estimates the half-maximal inhibitory concentration (IC50) values of drugs based on data from the Pharmacogenomics databases (https://www.cancerrxgene.org/) and the NCI-60 CellMiner database (https://discover.nci.nih.gov/cellminer/). To identify therapies targeting gene-mediated tumor promotion, we performed a cMAP analysis using the cMAP_gene_signatures.RData file, containing 1,288 compound-associated signatures. A gene signature of 150 significantly upregulated and 150 downregulated genes was derived from tumor expression data and compared to cMAP signatures using the XSum method. Compounds with lower similarity scores may inhibit gene-mediated cancer promotion following established protocols [21].

2.6 Analysis of single-cell RNA sequencing GSE141445

The data of GSE141445 were processed by the "Seurat" software package (v4.3.0) as follow procedures. Quality Control (QC): Removed low-quality cells (fewer than 200 detected genes) and genes (expressed in fewer than 3 cells). Cells with > 10% mitochondrial content were excluded to filter out apoptotic/damaged cells. Normalization: Applied LogNormalize to the filtered expression matrix. Dimensionality Reduction & Clustering: Used Principal component analysis (PCA) for dimensionality reduction and Louvain clustering (resolution = 0.5). Cluster Identification: Identified markers via FindMarkers and annotated clusters using CellMarker. Cell–Cell Interactions: Predicted ligand-receptor interactions with CellChat (v1.6.1). Visualization: Mapped clusters with Uniform Manifold Approximation and Projection (UMAP), and visualized model gene scores using AUCell.

2.7 Spatial transcriptomic analysis

Data processing steps for human prostate acinar cell carcinoma were as follows (10 × Genomics Visium, Seurat v4.3.0). Quality Filtering: Removed low-quality spots and artifacts—spots with < 200 or > 6,000 detected genes, > 10% mitochondrial content, and genes detected in < 3 spots. Normalization & Dimensionality Reduction: Used SCTransform for normalization, performed PCA on highly variable genes (HVGs) and selected the top 30 principal components (PCs) based on the elbow plot & JackStraw method. Applied UMAP for visualization. Spatial Clustering & Annotation: Louvain clustering (resolution = 0.5) was performed on PCA-reduced space. Marker genes were identified via the Wilcoxon rank-sum test (adjusted $p < 0.05$, log2FC > 0.25). Clusters were annotated using marker genes, spatial context, and Human Protein Atlas references. Visualization: H&E histology images were aligned with spatial transcriptomics data using Loupe Browser. Spatially variable genes were identified via SpatialDE, and AUC scores were used to assess gene set expression across microregions. SpatialFeaturePlot was applied for visualization.

2.8 Detection the levels of C11-BODIPY, Fe^{2+}, and ROS in cells overexpressing CD38 via flow cytometry

PCa cell line of PC-3 cells (Procell, Wuhan, China) are cultured in RPMI-1640 medium (Thermofisher, Massachusetts, USA) with 10% FBS (Thermofisher, Massachusetts, USA) and 1% Penicillin–Streptomycin (#60162ES76, Yeasen, Shanghai, China) under 95% air and 5% CO_2 at 37 °C. When the cell confluence reached 80%, CD38 overexpression plasmid (NewHelix, Shanghai, China) carried by Lipo3000 liposomes (#L3000001, Thermofisher, Massachusetts, USA) was added and cultured

for another 48 h. The probe kit of C11-BODIPY (#HY-D1301, MCE), 2′,7′-dichlorofluorescin diacetate (H2DCFDA, #HY-D0940, MCE), and FerroOrange (#GC19943, GLPBIO, Montclair, USA) were used to assess lipid peroxidation, ROS levels, and ferric ion content, respectively, following the manufacturer's instructions.

2.9 RNA extraction and reverse transcription real-time quantitative polymerase chain reaction (qRT-PCR)

Total RNA was isolated from the cells using an RNA extraction kit and then reverse-transcribed into cDNA with Reverse Transcriptase (#ENZ-KIT105-0050, Enzo, Shanghai, China) following the manufacturer's protocol. The resulting cDNA was used as a template for quantitative real-time PCR with SYBR Green PCR Master Mix (#Q711-02, Vazyme, Nanjing, China) and specific primers (Table S1). The PCR reactions were performed in a thermal cycler under optimized conditions, including an initial denaturation step, amplification, and melt curve analysis to verify product specificity. Each sample was analyzed in triplicate to ensure reproducibility and relative mRNA expression levels were determined using the 2^-ΔΔCt method. GAPDH served as the internal reference gene for normalization, ensuring accurate and reliable comparisons between samples.

2.10 Statistical analysis

All statistical analyses were performed using the R package (version 4.3.1). Group comparisons were conducted using the Wilcoxon test, while associations between variables were assessed using the Spearman correlation test. Survival analysis was performed using the Kaplan–Meier method, with group differences evaluated by the log-rank test. Multivariate and univariate analyses were conducted using the Cox proportional hazards model. Statistical significance was defined as $p < 0.05$, with significance levels denoted as follows: *$p < 0.05$, **$p < 0.01$, ***$p < 0.001$, and ****$p < 0.0001$.

3 Results

3.1 Machine learning guides the construction of prognostic models based on differential prognostic-associated genes shared by ferroptosis and fatty acid metabolism

The "limma" method was used to analyze the differential genes between prostate cancer and normal tissues in the TCGA dataset, and 73 common genes were obtained after intersection with genes related to ferroptosis and fatty acid metabolism (Fig. 1A). Subsequently, the univariate regression analysis method was used to identify genes related to biochemical recurrence of prostate cancer among the 73 genes. A total of 19 genes were identified, among which eight genes (PDK4, LTF, PTGS2, CD38, CAV1, LCN2, EGR1, P4HB) had a hazard ratio less than 1, which was a protective factor, and eleven genes (CYP4F8, RIPK3, AURKA, NOX4, TXN, CDKN2A, HPX, ALB, EZH2, APOE, APOC1) had a hazard ratio greater than 1, which was a risk factor (Fig. 1B). We then constructed a PPI network of genes. It showed that PTGS2 is closely related to other genes (Fig. 1C). Correlation analysis between genes found that APOE and APOC1 are most significantly correlated (Fig. 1D).

Based on the above 19 genes, we constructed a diagnostic model through 11 machine learning algorithms and 113 combinations of R packages, set the TCGA dataset as the training model, and set the DFKZ dataset as the validation model. We found that the combined algorithm of Lasso + RSF could obtain the best C index of 0.876 (Fig. 2A). The model contains a total of 12 genes ALB, APOE, AURKA, CD38, CYP4FB, EZH2, HPX, LCN2, NOX4, P4HB, PTGS2, RIPK3, and their coefficients were 0.5058, 3.872, 1.026, −1.046, 0.9769, 0.7990, 0.2547, −0.4549, −0.2039, 0.5240, 0.1448, 1.2498, respectively. Survival analysis found that the prognosis of the high-risk group in our model was worse than that of the low-risk group (Fig. 2B). ROC curve analysis found that the 1-, 2-, and 3-year prediction efficiencies of the prediction model were 0.77, 0.75, and 0.78, respectively (Fig. 2C). The results obtained from the validation cohort-DFKZ indicating the reliability of the model (Fig. 2D, E). Results of the independent analysis conducted by univariate and multivariate Cox regression showed that the risk model can predict biochemical recurrence of prostate cancer independently of other clinical characteristic indicators such as age, stage, and Gleason score (Fig. 2F, G). Similar results were obtained from the validation cohort (Fig. 2H, I). Subsequently, we compared the differences in risk scores among patients with different clinical characteristics. The risk score was higher in patients older than 65 years, higher in patients with a Gleason score greater than 7, and increased with increasing T stage (Fig. 3A). This indicates that the risk score is closely related to clinical characteristic factors. To increase the clinical translatability of the risk score, we constructed a nomogram scoring tool that includes risk score, TNM stage, age, and other factors (Fig. 3D). The calibration curves show that the nomogram can accurately predict 1, 2, and

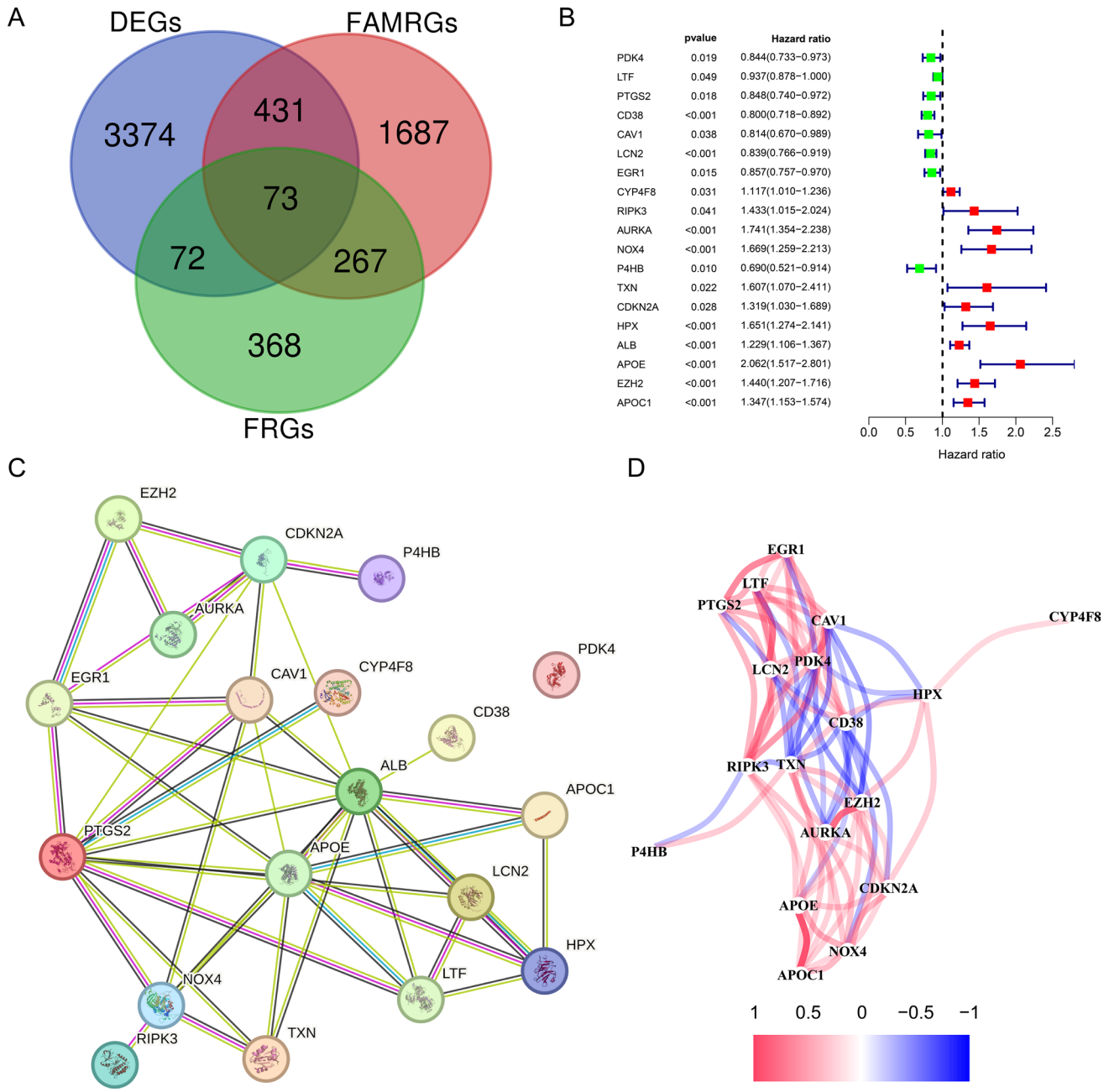

Fig. 1 Identification of prognostic common genes between the DEGs, FAMRGs, and FRGs. **A** Venn diagram displayed the common genes of DEGs, FAMRGs, and FRGs. **B** Identification of prognostic genes derived from the common genes via univariate Cox analysis. **C** Construction of a PPI network from the STRING database. **D** Correlation network of the generated prognostic genes. The bluer the color, the stronger the negative correlation, and the redder the color, the stronger the positive correlation

3-year PFS, and the and decision curves show that its combined decision performance is better than that of the individual risk score and clinical characteristic factors (Fig. 3B, C). These results indicated that the model built based on machine learning can reliably and stably predict PFS of prostate cancer, and could provide an effective tool for clinical practice.

3.2 Functional annotation of potential biological pathways

To investigate the underlying reasons for the observed differences between the high-risk and low-risk groups, we employed the "clusterProfiler" package to analyze pathways enriched by differentially expressed genes (DEGs) in these groups. Gene Ontology (GO) analysis revealed that the DEGs were primarily associated with immune-related pathways,

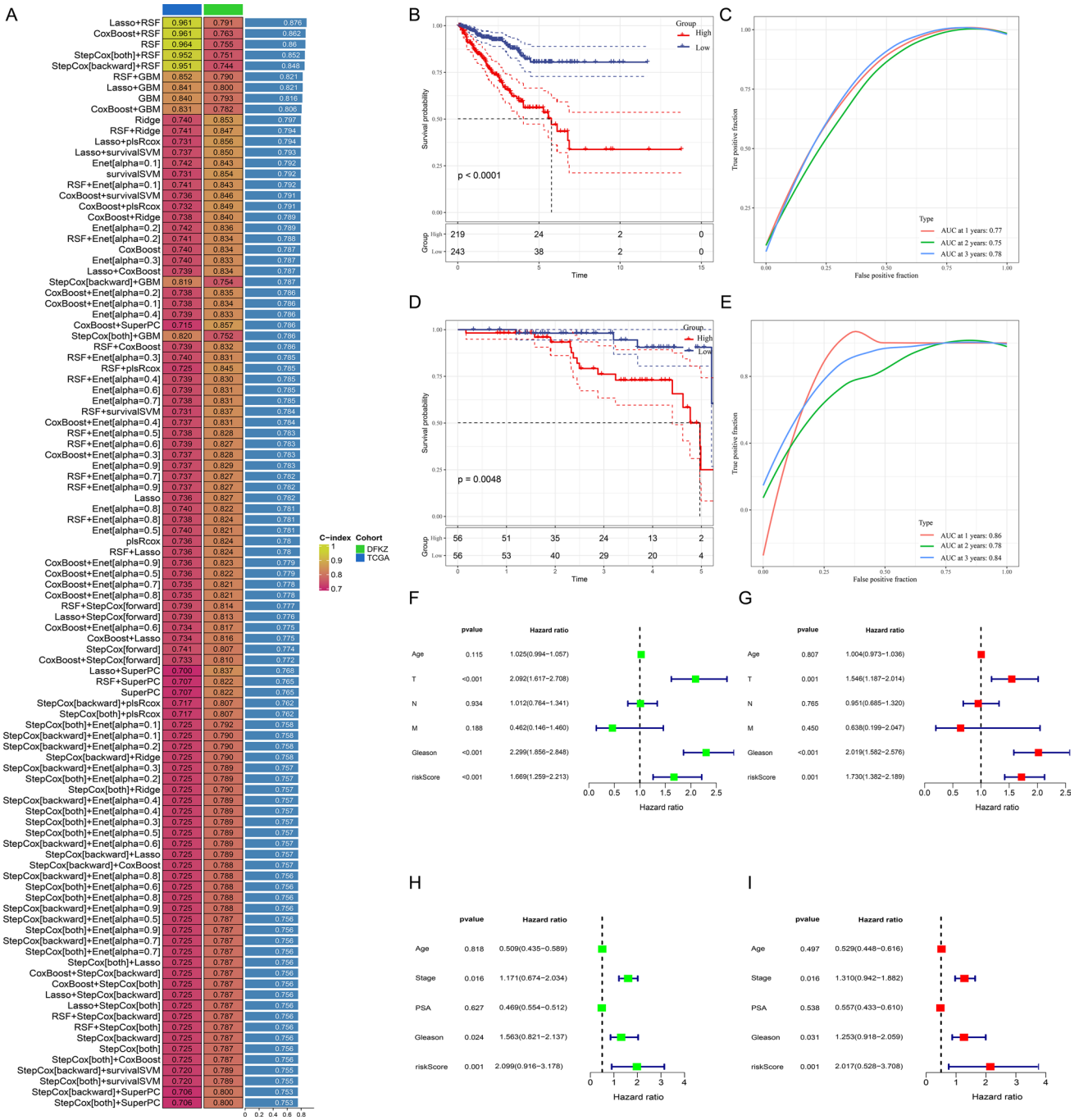

Fig. 2 Construction and validation of a prognostic model via machine learning methods. **A** Mean values of C-index values calculated by machine learning methods in the TCGA and DFKZ cohorts. **B**, **D** PFS survival curves of the high- and low-risk group in the TCGA and DFKZ cohorts, respectively. **C**, **E** ROC curves at 1-, 2-, and 3-years of TCGA and DFKZ cohorts, respectively. **F**, **G** Univariate and multivariate Cox regression analysis of Age, TNM stage, Gleason score, and risk score in the TCGA cohort. **H**, **I** Univariate and multivariate Cox regression analysis of Age, stage, Gleason score, PSA, and risk score in the DFKZ cohort

including the production of immune response molecular mediators, immunoglobulin complexes, and antigen-binding (Fig. 4A). Similarly, Kyoto Encyclopedia of Genes and Genomes (KEGG) enrichment analysis indicated that the DEGs were enriched in signaling pathways such as the cell cycle, cytokine-receptor interactions, TGFβ signaling, and NF-κB signaling (Fig. 4B). Furthermore, Gene Set Enrichment Analysis (GSEA) was conducted to examine pathways from the Hallmark collection. In the high-risk group, the top five enriched pathways included allograft rejection, E2F targets, G2M checkpoint, mitotic spindle formation, and spermatogenesis (Fig. 4C). In contrast, pathways such as androgen response,

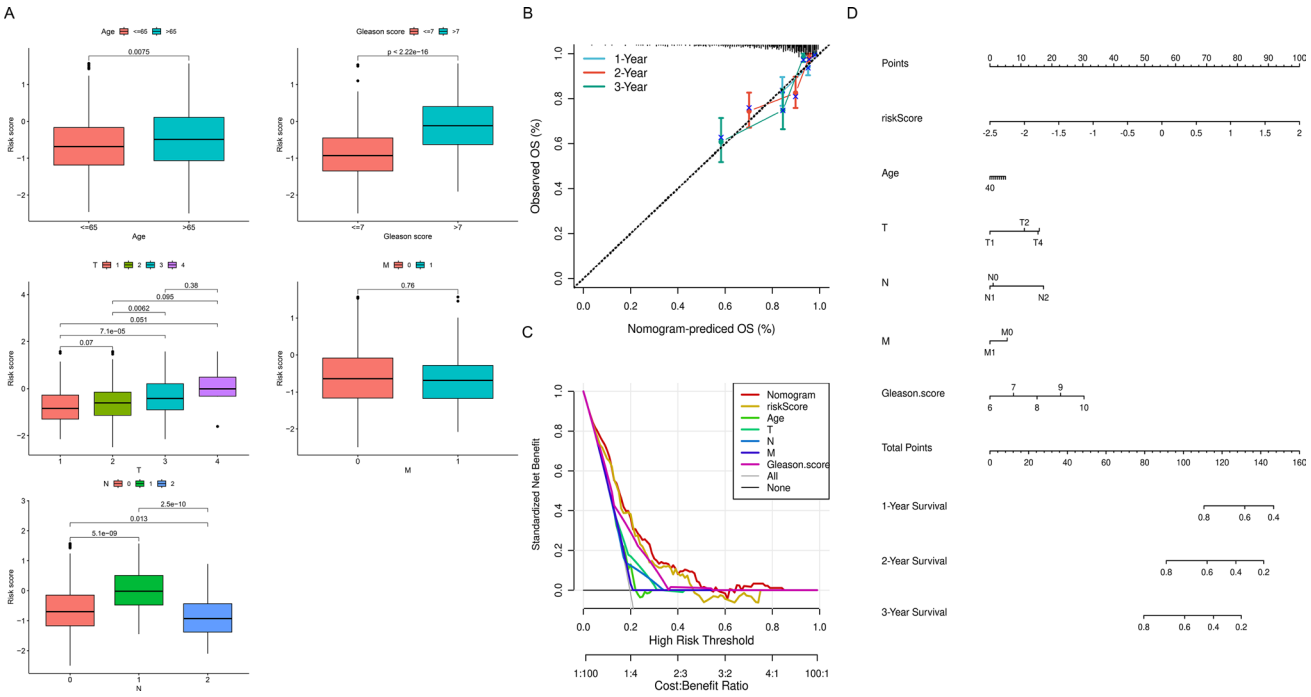

Fig. 3 Building and evaluating a nomogram integrated clinical factors and risk score. **A** Comparison of risk scores across different clinical characteristics. **B**, **C** The predicted ability of the nomogram was estimated by calibration curves (**B**) and decision curves (**C**). **D** Based on clinical factors such as age, TNM stage, Gleason score, and risk score, a nomogram score table was constructed to predict the 1-, 2- and 3-year PFS of prostate cancer patients

apical surface, cholesterol homeostasis, protein secretion, and reactive oxygen species were predominantly enriched in the low-risk group (Fig. 4D). Correlation analysis demonstrated that several key model genes, including CD38, RIPK3, LCN2, PTGS2, APOE, and NOX4, exhibited significant positive correlations with the majority of the Hallmark pathways, indicating their potential involvement in various oncogenic and immunological processes (Fig. S1). These genes may contribute to critical cellular mechanisms such as inflammation, immune response regulation, metabolic pathways, and tumor progression. For instance, CD38 and RIPK3 have been linked to immune cell activation and programmed cell death, while LCN2 and PTGS2 play essential roles in inflammation and tumor microenvironment remodeling. Conversely, the remaining model genes demonstrated negative correlations with most Hallmark pathways, suggesting their potential roles in tumor suppression or resistance to specific signaling cascades. These negative associations may indicate their involvement in pathways that inhibit cancer progression or regulate immune evasion. Collectively, these findings provide valuable insights into the functional landscape of the model genes and their potential implications for tumor biology and therapeutic interventions.

3.3 Analysis of tumor mutations in the two groups of PCa patients

Tumors are characterized by abnormal and uncontrolled cell growth caused by gene mutations, which can affect pathway changes leading to tumor progression [22]. Therefore, we analyzed the differences between high-risk and low-risk groups from the perspective of tumor mutation burden. We initially explored the mutation landscape of PCa, revealing distinct patterns of genetic alterations. Missense mutations constituted the largest proportion of observed mutations (Fig. S2A). Single nucleotide polymorphisms (SNPs) were more frequent than insertions and deletions (Fig. S2B), with C > T transitions being the most prevalent type of single nucleotide variant (SNV) (Fig. S2C). An analysis of the number of altered bases per patient showed a median mutation count of 21 (Fig. S2D). Box plots illustrated the occurrence frequency for each variant category and also suggested that missense mutations are most frequent in PCa (Fig. S2E). The oncoplot for the top ten genes with somatic nucleotide variations in PCa indicated that TTN (13%) had the highest mutation frequency, followed by TP53 (11%), SPOP (11%), KMT2D (6%), MUC16 (5%), SYNE1 (5%), FOXA1 (6%), KMT2C (4%), LRP1B (4%), and SPTA1 (4%) (Fig. S2F). Subsequently, we analyzed the Copy number variation (CNV) frequency of model genes, it indicated that the model genes were relatively stable in PCa,

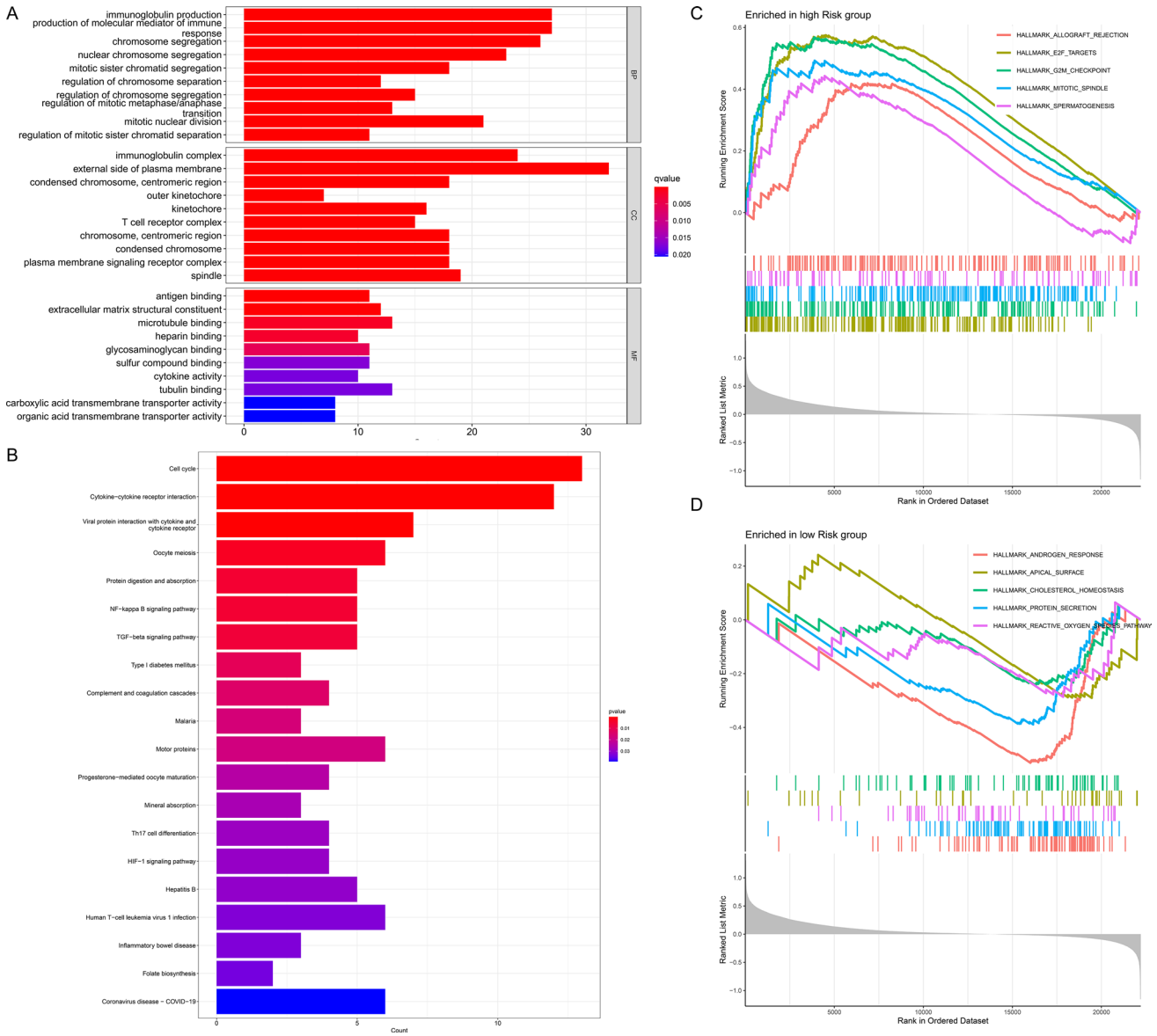

Fig. 4 Potential mechanisms were analyzed by functional enrichment. **A** GO enrichment analysis. **B** KEGG enrichment analysis. **C**, **D** Hallmark enrichment analysis in the high- and low-risk groups

and the CNV frequency is low, not exceeding 4%. The top five genes with higher frequencies are EZH2, APOE, P4HB, LCN2, and PTGS2 (Fig. 5A). The TMB scores were calculated and compared, and it showed that the TMB scores in the high-risk group were much higher than that in the low-risk group ($p < 0.0001$, Fig. 5B), and showed strong positive association with risk scores ($cor = 0.24$, $p < 0.0001$, Fig. 5C). Gene mutations in tumors often cause pathway activation or inhibition, thereby affecting tumor progression and treatment outcomes [23, 24]. The top 10 most affected pathways are illustrated in Fig. 5D. Among these, the RTK-RAS pathway exhibited the highest proportion of affected samples in both high-risk and low-risk groups; however, the proportion was significantly higher in the high-risk group (57/85, the right panel). Similarly, other pathways, including NOTCH, WNT, and Hippo, showed a higher proportion of affected samples in the high-risk group. This trend was corroborated by the mutation landscape analysis, which revealed a substantially higher proportion of gene mutations in high-risk patients (67.76%, the right panel) compared to those in the low-risk group (48.54%, the left panel) (Fig. 5E). Additionally, the top 15 most frequently mutated genes were identified and compared between the two groups. In the low-risk group, TTN emerged as the most frequently mutated gene (10%), while its mutation frequency in the high-risk group was slightly lower (9%). Conversely, the mutation frequency of TP53 was markedly higher in the high-risk group (17%) compared to the low-risk group (3%).

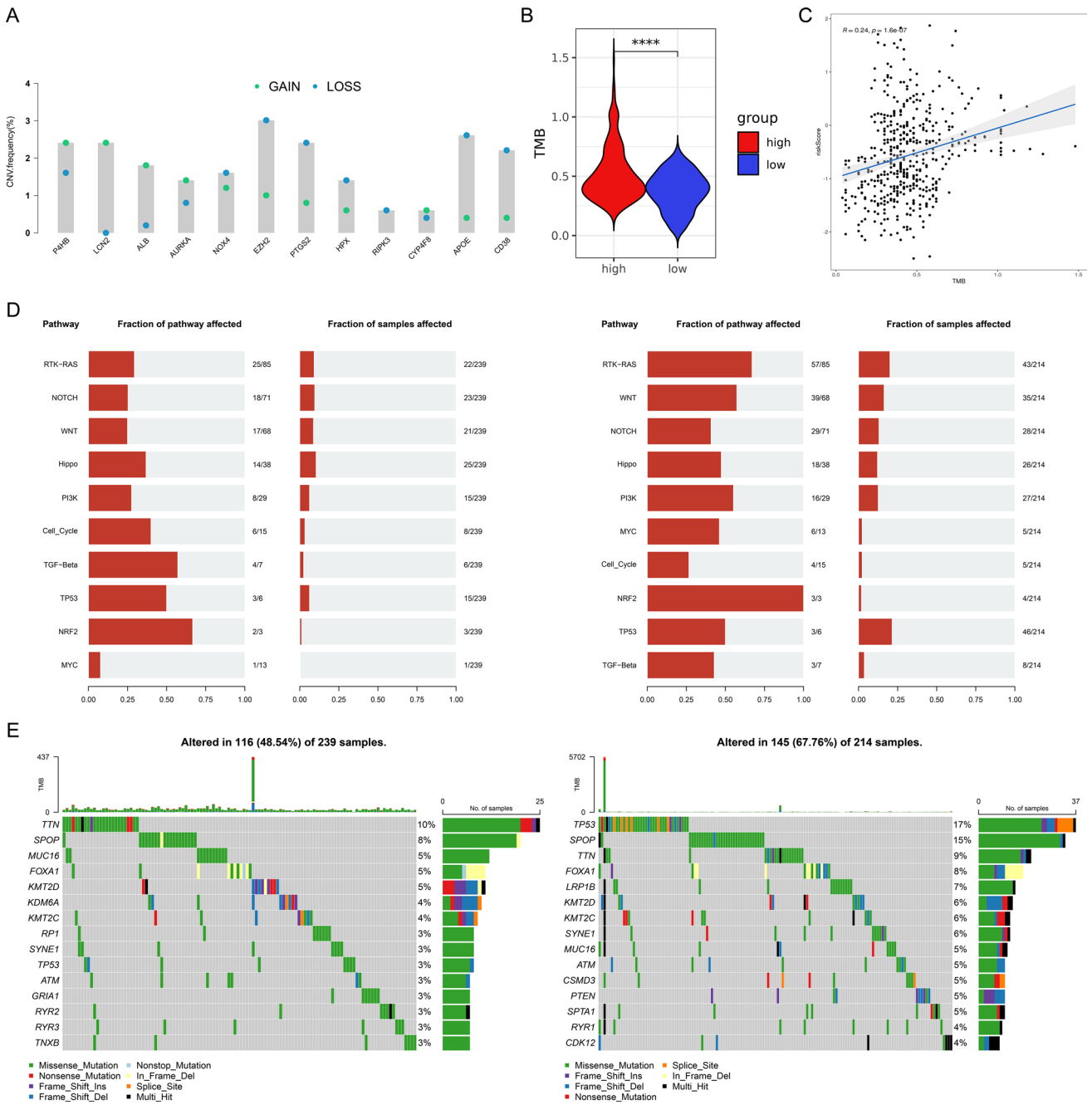

Fig. 5 Differences in tumor mutation burden between high- and low-risk groups. **A** The difference in TMB score among the two groups. **B** The CNV frequency of model genes. **C** The top 10 pathways most significantly affected by mutations in the low- (left) and high-risk (right) groups. **D** The top 15 most frequent genes in the low- (left) and high-risk (right) groups. ****$p < 0.0001$. **E** The top 15 genes with thehighest mutation frequencies in the high-risk and low-risk groups

These findings underscore pronounced differences in the mutational landscape between high-risk and low-risk groups, further highlighting the molecular heterogeneity underlying these classifications.

3.4 Immune cell infiltration and immunotherapy response among the two groups

To further explore the differences between the high-risk and low-risk groups, we conducted an in-depth analysis of the immune microenvironment. Comparisons of the stromal score, immune score, and ESTIMATE score revealed that all three scores were significantly higher in the high-risk group than in the low-risk group, suggesting heightened

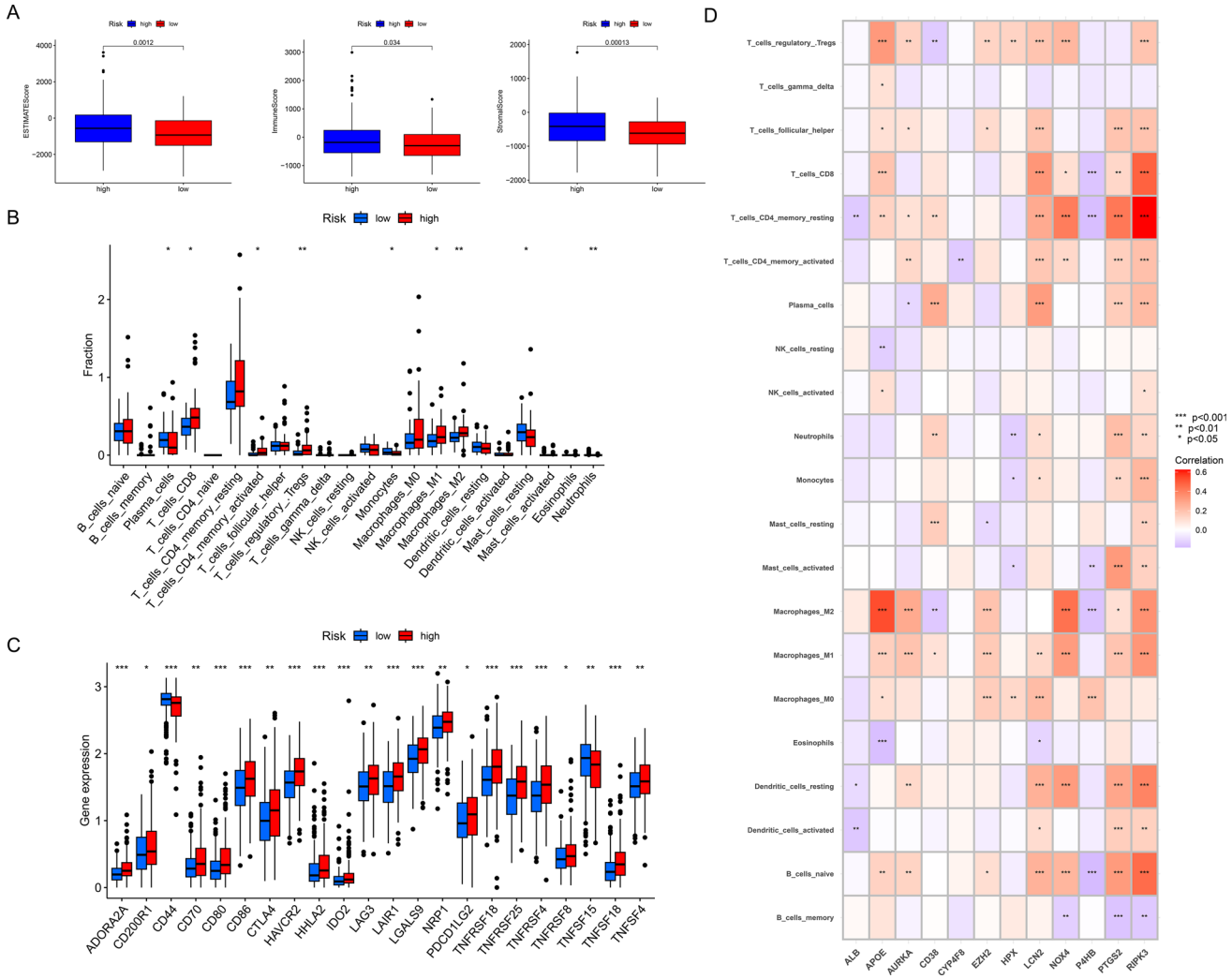

Fig. 6 Estimation of immune cell infiltration among the two groups. **A** Differences of Estimate, immune, and stromal scores calculated by ESTIMATE method. **B** Differences in different immune cell populations between the two groups were evaluated via the CIBERSORT algorithm. **C** Differences in different immune checkpoints between the two groups. **D** Correlation analysis between model genes and infiltration levels of different immune cell subsets. The bluer the color, the stronger the negative correlation, and the redder the color, the stronger the positive correlation. *p < 0.05, **p < 0.01, ***p < 0.001, ****p < 0.0001

immune-related activity in the high-risk group (Fig. 6A). Immune cell population analysis, as shown in Fig. 6B, revealed distinct infiltration patterns between the groups. Specifically, CD8 + T cells, activated memory CD4 + T cells, regulatory T cells, and macrophages (M1 and M2) exhibited higher levels of infiltration in the high-risk group. In contrast, plasma cells, monocytes, and neutrophils were more prominently infiltrated in the low-risk group. We also observed that key immune checkpoints—including PDCD1LG2 (CD273), CTLA-4, HAVCR2, and LGALS9—were significantly upregulated in the high-risk group. This heightened expression likely contributes to fostering an immunosuppressive tumor microenvironment, which may facilitate immune evasion (Fig. 6C). Additionally, the model genes demonstrated significant correlations with various immune cell types. It showed that APOE was strongly associated with M2 macrophages, while RIPK3 showed significant correlations with quiescent memory CD4 + T cells and CD8 + T cells. Interestingly, CD38 was negatively correlated with M2 macrophages and positively correlated with M1 macrophages (Fig. 6D). These findings indicate that immune microenvironmental differences may contribute to the observed disparities in PFS between the high-risk and low-risk groups of PCa patients.

Immunotherapy treated by immune checkpoint inhibitors (ICI) has emerged as a promising treatment modality for a variety of cancers, including PCa, but its efficacy against this malignancy has been more difficult to determine, and we explored whether models could provide guidance for personalized treatment. The high-risk group exhibited significantly

higher TIDE scores ($p < 0.01$), MSI scores ($p < 0.001$), exclusion scores ($p < 0.05$), and dysfunction scores ($p < 0.01$), while a higher TIDE score correlates with a poorer response to immunotherapy, suggesting a greater likelihood of immune evasion and resistance to ICI therapy (Fig. 7A). In the Imvigor210 dataset, we observed that the risk scores of patients who responded to ICI therapy, including those with complete response (CR) and partial response (PR), were lower than those of non-responsive patients, categorized as having stable disease (SD) or progressive disease (PD) ($p < 0.0001$, Fig. 7B). In the high-risk group, 16% of patients responded to treatment, while in the low-risk group, 30% of patients responded to treatment (Fig. 7C). Furthermore, regardless of whether patients were in the early or late stages of the disease, those patients with lower risk scores demonstrated a longer survival tiem (Fig. 7D). These results further suggest that patients in the low-risk group are more likely to benefit from immunotherapy, which also provides a basis for personalized treatment.

3.5 Prediction of chemotherapy and discovery of potential small molecules

Chemotherapy is also a conventional method for treating PCa, but it is not effective for all patients, so it is necessary to classify and screen patients who may respond to treatment. Our analysis revealed that the IC50 values of 5-Fluorouracil,

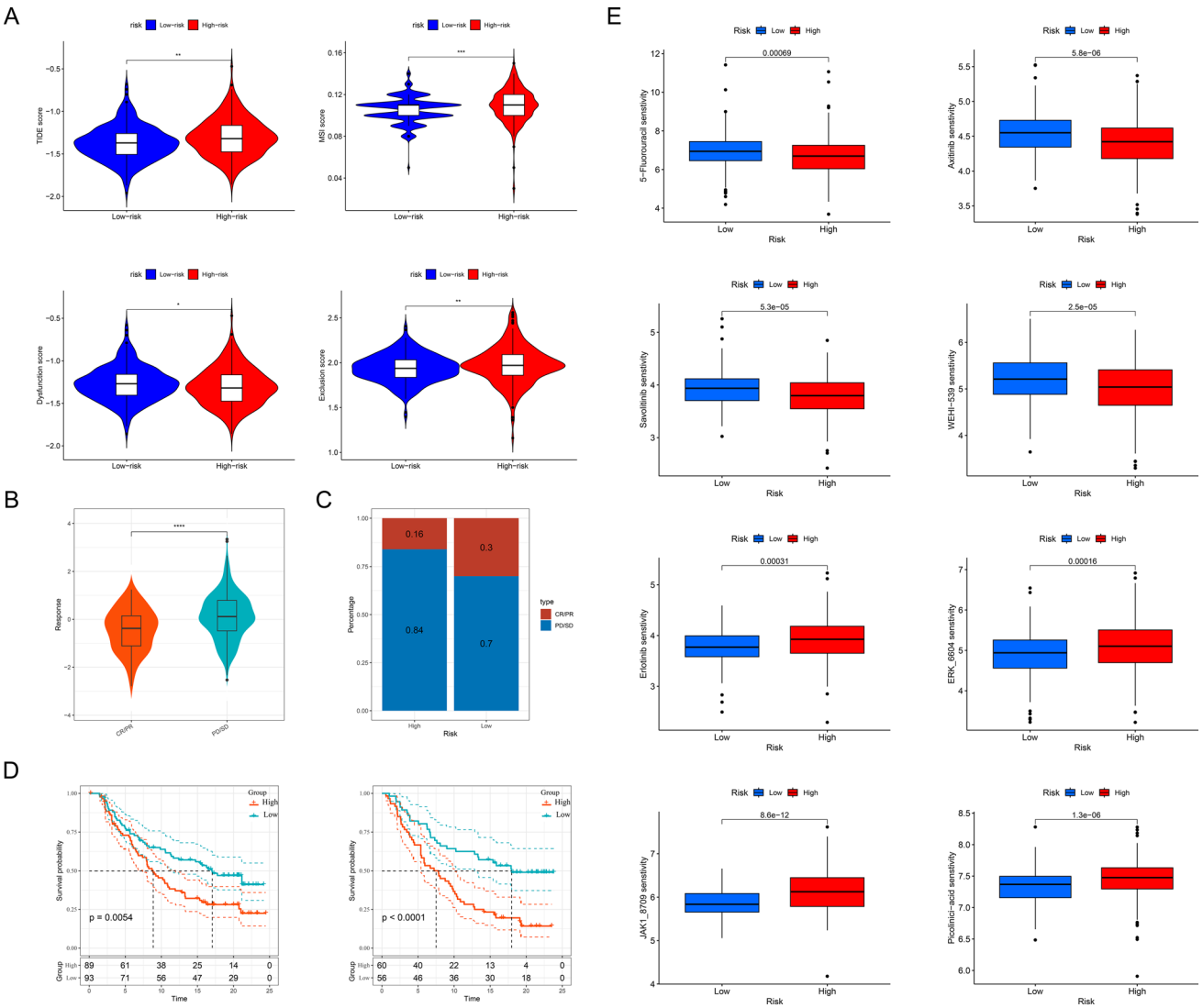

Fig. 7 Prediction of immunotherapy response and chemotherapy drug sensitivity. **A** Differences in TIDE, MSI, dysfunction, and exclusion scores were calculated by the TIDE method. **B** Differences in scores between responding and non-responding patients. **C** Distribution of the proportion of responding and non-responding patients between high-risk and low-risk groups. **D** Survival analysis of patients with early (stages of I + II, the left panel) and advanced (stages of III + IV, the right panel) stages in the two groups. **E** Differences in drug sensitivity between the two groups. *$p < 0.05$, **$p < 0.01$, ***$p < 0.001$, ****$p < 0.0001$

Savolitinib, Axitinib, and WEHI-539 were significantly higher in the low-risk group, suggesting that patients in this group may exhibit reduced sensitivity to these four drugs. Conversely, the lower IC50 values observed for Erlotinib, ERK_6604, JAK1_8709, and Picolinic acid in the low-risk group indicate a potentially heightened sensitivity to these agents (Fig. 7E). The analysis of the CellMiner dataset provided valuable insights into the relationship between gene expression and drug sensitivity, highlighting potential therapeutic implications. Specifically, CD38 expression levels were positively correlated with the IC50 values of multiple drugs, including Nelarabine, Fluphenazine, XK-469, and Ifosfamide, suggesting that higher CD38 expression may be associated with reduced sensitivity to these agents. In contrast, CD38 expression exhibited a negative correlation with the IC50 of Irofulven, indicating that tumors with elevated CD38 expression might be more responsive to this drug. Additionally, PTGS2 expression showed an inverse correlation with the IC50 of Vincristine, implying that higher PTGS2 levels could enhance sensitivity to this chemotherapeutic agent. Meanwhile, HPX expression was positively correlated with the IC50 of SR16157, suggesting a potential role in modulating drug resistance (Fig. S3A). The XSum algorithm, leveraging the cMAP database, identifies potential small molecules and drugs capable of mitigating the biological effects arising from dysregulated target gene expression [21]. According to this analysis, the small molecule X4.5-dianilinophthalimide was identified as a potential therapeutic agent for PCA, as it may regulate the biological effects associated with the dysregulated expression of AURKA, CD38, and EZH2. Additionally, PHA.00816795 was suggested to counteract the effects induced by the dysregulated expression of LCN2 and RIPK3 (Fig. S3B).

3.6 Exploring the relationship between risk score and cell distribution via sc-RNA and spatial transcriptomics

Single-cell technology offers a powerful tool to elucidate the spatial distribution of genes and the intricate communication networks between different cell types. To gain deeper insights into the relationship between the established scoring model and prostate cancer, we conducted an in-depth analysis of the GSE141445 dataset. This approach allowed us to explore the molecular and cellular dynamics associated with the disease, further bridging the scoring model to underlying biological mechanisms. After dimensionality reduction processing with the Seurat package, 8 types of cells were annotated, including B cells, exhausted CD8 T cells (CD8 Tex), endothelial cells, epithelial cells, fibroblasts, malignant cells, mast cells, and macrophage. The malignant cells were the most abundant group (Fig. 8B). The three most significantly up-regulated and down-regulated genes in each cell type are shown in fan-shaped graphs (Fig. 8A). The number and intensity of interactions among all cell types in PCa samples were comprehensively analyzed and systematically summarized via Cellchat, providing an in-depth overview of the cellular communication landscape within the tumor microenvironment (Fig. 8C). Each type of cell is shown separately, and it is found that epithelial cells and macrophages have relatively strong communication with other cells (Fig. 8D). It highlights the intricate network of cell–cell interactions and their potential roles in shaping tumor progression. The primary outgoing and incoming signaling patterns of each cell group were illustrated in Fig. 8E, macrophages had higher intensities in both input and output signaling models, suggesting that they may play a major role in the PCa microenvironment. We applied the AUCell method to calculate the distribution of the risk scores. We found that stromal cells and malignant cells scored higher than immune cells and higher immune cell risk scores were mainly distributed in macrophages, followed by epithelial cells and malignant cells (Fig. 8F–H). The expression profiles of the model genes were thoroughly examined, revealing distinct patterns across various cell types. Specifically, AURKA, ALB, RIPK3, EZH2, NOX4, and CD38 were expressed at relatively low levels, whereas P4HB exhibited widespread expression across multiple cell types. Notably, APOE was predominantly localized in macrophages, while PTGS2 was primarily expressed in mast cells (Fig. 8I). These findings provide valuable insights into the cell-type-specific roles of these genes within the tumor microenvironment.

Spatial transcriptomics technology offers a critical spatial context for gene expression, enabling a deeper understanding of the spatial organization within tissues [25]. Using this advanced approach, we further investigated the spatial distribution of model genes and their associated scores. The location of 11 cell types including plasma cells, CD4 T cells, CD8 T cells, dendritic cells (DCs), endothelial cells, epithelial cells, fibroblasts, macrophages, neutrophil, natural killer cells (NK cells), and tumor cells was depicted. The estimated scores were major found in the macrophage, but not tumor cells, it was consistent with the results from the single-cell results (Fig. 9). Furthermore, the localization of model genes and their associations with specific cell subpopulations were examined in detail. P4HB was found to be broadly expressed across the entire tissue section, showing a strong positive correlation with tumor cells. APOE was detected at low expression levels across the tissue sections, with its distribution showing a positive correlation with CD4 + T cells, natural killer (NK) cells, and macrophages. In contrast, a negative correlation was observed between APOE expression and DCs. Interestingly, in contrast to the single-cell analysis results, LCN2 exhibited high expression levels in macrophages, endothelial

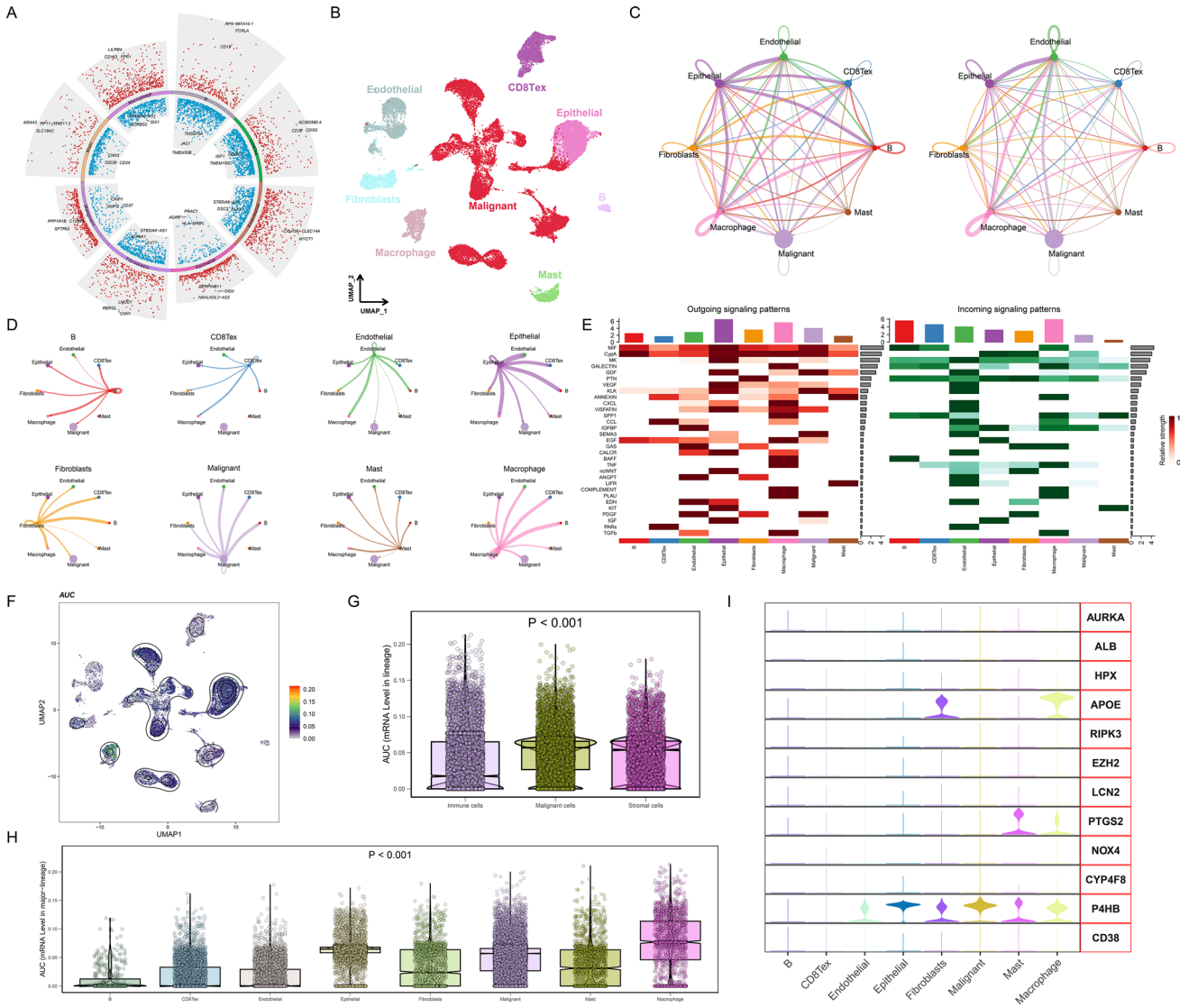

Fig. 8 Exploring the relationship between risk score and cell distribution via sc-RNA analysis. **A** Identifying specific markers for different cell types. **B** Different cell types in the GSE141445 dataset are shown in the UMAP plot. **C** Weight and count of cell chat network. **D** The communication network of each cell type with other cells. **E** The incoming and outgoing pathways. **F** Explore the distribution of model scores across different cell populations via the AUCell function shown by UMAP. **G** Distribution of model scores in the main cell types. **H** Distribution of model scores inthe various specific cell types. **I** Distribution of model genes in the sc-RNA sequencing

cells, and DCs (Fig. S4). These findings offer valuable insights into the spatial expression patterns and potential functional roles of these genes within the prostate cancer microenvironment, highlighting their contributions to the complexity of tumor biology.

3.7 Overexpression of CD38 induces ferroptosis in prostate cancer cells

CD38 plays a crucial role in tumors by regulating immune responses and tumor microenvironment. It enhances immunosuppressive pathways, promotes tumor growth, and inhibits immune surveillance [26, 27]. CD38 is involved in the metabolism of NAD + and modulates cellular processes critical for prostate cancer progression, such as proliferation and DNA repair [28, 29]. Targeting CD38 has emerged as a promising strategy in cancer therapy, influencing immune cell function and tumor viability. Interestingly, we observed a decrease in CD38 expression in prostate cancer tissues, and its association with ferroptosis and fatty acid metabolism has not been previously reported, which piqued our interest. The plasmid was successfully delivered using Lipo3000 liposomes, leading to increased CD38 expression in PC-3 cells

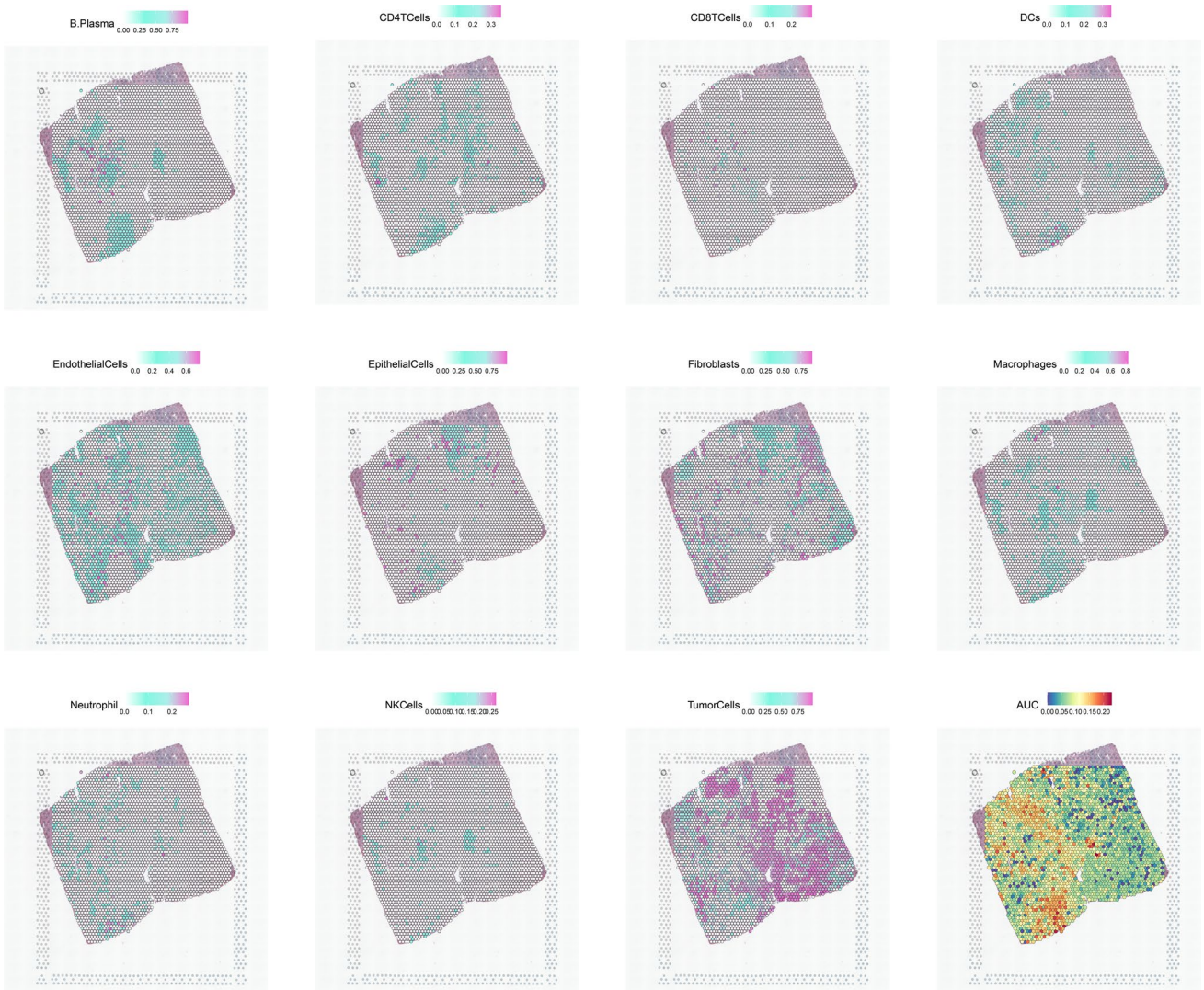

Fig. 9 Exploring the relationship between risk score and cell distribution via spatial transcriptomics. Visualizing risk scores through spatial transcriptome, distribution of different cells, and risk scores in the slice

(Fig. 10A). However, the analysis revealed that while CD38 overexpression did not affect fatty acid metabolism (data not shown), it significantly altered ferroptosis-related indicators. The ferroptosis inhibitors glutathione peroxidase 4 (GPX4) and solute carrier family 7 member 11 (SLC7A11) were significantly downregulated, while the ferroptosis marker prostaglandin synthase 2 (PTGS2) was markedly upregulated, indicating that the cells underwent ferroptosis (Fig. 10B). Additionally, intracellular lipid peroxidation (C11-BODIPY) and ROS levels were elevated in CD38-overexpressing cells, while the FerroOrange probe indicated an increase in intracellular iron content (Fig. 10C). These findings further support that CD38 overexpression induces ferroptosis.

4 Discussion

This study integrated ferroptosis and fatty acid metabolism (FAM)-associated genes to construct a robust prognostic model for PCa using machine learning. A Lasso + RSF-based model achieved a high C-index of 0.876 and demonstrated reliable 1-, 2-, and 3-year predictive accuracy (AUCs: 0.75–0.78). The model's risk score correlated with clinical characteristics (age, Gleason score, T stage) and was validated in an independent cohort. Functional annotation revealed distinct pathway activities: high-risk groups were enriched in immune and proliferative pathways (G2M checkpoint), while low-risk groups showed metabolic stability (androgen response, cholesterol homeostasis). Tumor mutation burden

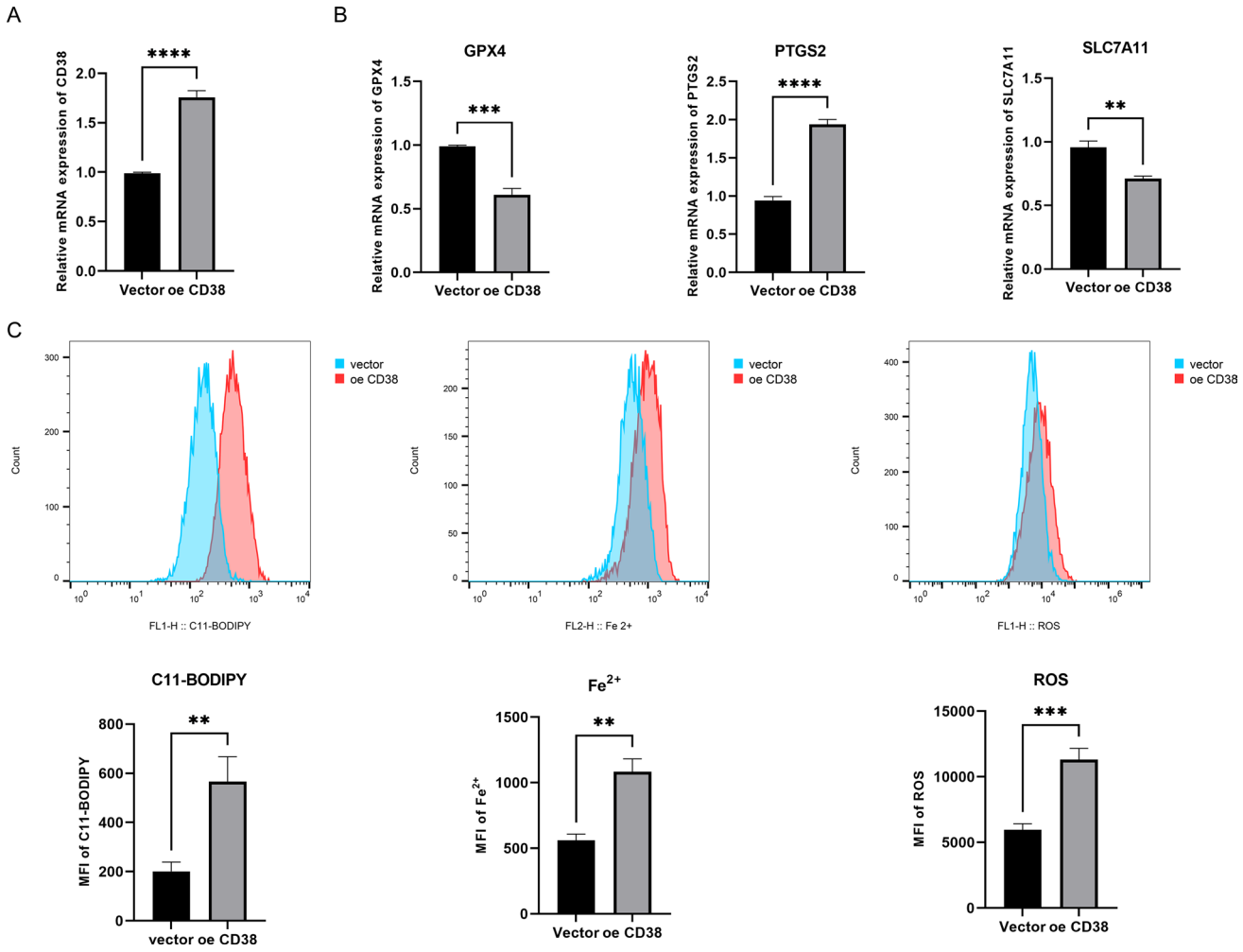

Fig. 10 CD38 contributes to ferroptosis of PC-3 cells. **A** Relative mRNA level of CD38. **B** Relative mRNA level of ferroptosis markers GPX4, PTGS2, and SLC7A11, respectively. **C** Detection of C11-BODIPY, Fe^{2+}, and ROS, respectively. **p < 0.01, ***p < 0.001, ****p < 0.0001

was significantly higher in high-risk groups, with TP53 mutations more prevalent. Immune cell infiltration analysis indicated heightened immune activity in high-risk groups, particularly CD8 + T cells and macrophages, while low-risk groups exhibited higher plasma cell infiltration. Immunotherapy response analysis suggested low-risk patients were more likely to benefit from immune checkpoint inhibitors. Additionally, chemotherapy sensitivity and potential small-molecule therapeutics were identified, with drugs like Erlotinib showing promise for low-risk patients. Single-cell and spatial transcriptomics revealed cell-type-specific gene expression patterns, highlighting macrophages and epithelial cells as key players in the tumor microenvironment. These findings underscore the model's potential for guiding personalized treatment and improving PCa prognosis.

The integration of ferroptosis- and FAM-related genes into prostate cancer prognostic models represents a significant departure from existing approaches, which typically focus on single pathways or universal genomic signatures. Our model, constructed using 19 differentially expressed genes shared between ferroptosis and FAM, demonstrated robust predictive performance (C-index = 0.876), outperforming traditional models reliant on clinical parameters like Gleason score or PSA levels, which typically yield C-indexes of 0.65–0.75 [30, 31]. Furthermore, our model's time-dependent AUCs (0.75–0.78) surpass those of recent multi-gene panels, such as the Decipher genomic classifier, which reports AUCs of 0.68–0.72 for biochemical recurrence prediction [32]. This highlights the advantage of incorporating pathway-specific insights into prognostic modeling. We employed 113 combinations of 11 machine learning methods to identify the optimal model, concluding that our framework (Lasso + RSF) represents a significant advancement over previous approaches. While earlier studies employed single algorithms like Cox regression or random survival forests, our combinatorial approach optimized feature selection and non-linear risk estimation, achieving higher predictive accuracy

compared to traditional models [33]. The nomogram's superior clinical utility over standalone risk scores or clinical factors echoes trends in precision oncology, where integrative tools like the CAPRA-S score have shown value but lack pathway-specific insights [34]. While our model's performance is promising, limitations exist. The overlap with prior multi-gene signatures remains unexamined, and external validation in ethnically diverse cohorts is needed [35]. Nevertheless, our findings bridge ferroptosis, FAM, and immune dysregulation—a triad increasingly recognized in cancer metabolism but rarely modeled cohesively. This work expands the translational potential of pathway-based machine learning models in prostate cancer, offering a template for other malignancies driven by metabolic-immune interplay. Despite the boom in machine learning, significant challenges remain in medical practice. Processing sensitive health data creates data privacy risks, and anonymization is often insufficient to prevent re-identification. Informed consent is complicated by data reuse beyond the scope of the initial patient agreement. Algorithmic bias stems from non-representative datasets and can lead to misdiagnosis or unequal care (e.g., racial disparities in diagnosis). Future directions prioritize privacy-preserving techniques (e.g., federated learning), dynamic consent models, bias mitigation through diverse data management, and explainable AI (XAI) for clinical transparency. Integrating ethics into ML development ensures fair, patient-centered innovation.

Key genes in our model, such as PTGS2, APOE, and APOC1, align with emerging evidence linking inflammation, lipid metabolism, and prostate cancer progression. PTGS2 (COX-2), a known mediator of ferroptosis and inflammation, has been implicated in prostate cancer aggressiveness, consistent with its protective role here (HR < 1) [36]. Conversely, APOE/APOC1, central to lipid transport, were identified as risk factors (HR > 1), corroborating studies linking dysregulated cholesterol metabolism to prostate cancer recurrence [37]. The strong correlation between APOE and APOC1 further supports their cooperative role in lipid signaling, as observed in Alzheimer's, though their interaction in cancer remains underexplored [38]. Functional analyses revealed distinct immune and proliferative pathway activities between risk groups. The enrichment of allograft rejection, E2F targets, and G2M checkpoint pathways in high-risk patients mirrors findings in immunogenic tumors, suggesting a paradoxical interplay between immune activation and treatment resistance [39]. Conversely, low-risk group pathways (androgen response, cholesterol homeostasis) align with studies showing favorable outcomes in tumors retaining hormonal sensitivity and metabolic stability [40]. The integration of single-cell RNA sequencing and spatial transcriptomics has provided unprecedented insights into the cellular heterogeneity and spatial organization of the PCa microenvironment. Our analysis of the GSE141445 dataset revealed distinct cell-type-specific gene expression patterns and intercellular communication networks, which are critical for understanding the molecular mechanisms underlying PCa progression and treatment resistance. Our study identified eight major cell types, with malignant cells being the most abundant, consistent with previous findings that luminal epithelial cells are the primary origin of PCa [41, 42]. Notably, macrophages exhibited strong communication with other cell types, particularly epithelial cells, highlighting their central role in shaping the TME. This aligns with recent studies showing that tumor-associated macrophages (TAMs) promote immunosuppression and therapy resistance in PCa [43]. The spatial transcriptomics analysis further validated these findings, revealing that risk scores were predominantly associated with macrophages rather than tumor cells. This suggests that macrophages may serve as key mediators of risk stratification in PCa, potentially through their interactions with other immune and stromal cells [43, 44]. The Cellchat analysis revealed intricate communication networks, with macrophages playing a pivotal role in both incoming and outgoing signaling. This aligns with recent studies demonstrating that macrophages mediate immunosuppression through pathways such as adenosine signaling, which can be targeted to enhance immunotherapy efficacy [43]. Additionally, the strong interaction between epithelial cells and macrophages suggests that targeting these interactions could disrupt tumor progression and improve treatment outcomes. Our findings are consistent with recent advancements in single-cell and spatial transcriptomics. For example, studies have highlighted the role of club-like cells in mediating immunosuppression and therapy resistance in PCa, further emphasizing the importance of epithelial-immune interactions [45]. Additionally, the identification of APOE + TAMs as key mediators of immunotherapy resistance in metastatic castration-resistant PCa (mCRPC) supports our observation that macrophages are central to risk stratification and treatment response [46, 47]. In tumor microenvironments, APOE can paradoxically support immunosuppression by skewing macrophages toward an M2-like phenotype. M2 macrophages are known to secrete factors like TGF-β and CXCL1, which dampen cytotoxic T-cell responses and promote angiogenesis [48]. APOE's lipid-shuttling function may further fuel tumor-associated macrophages (TAMs) to adopt a pro-tumorigenic state, facilitating immune evasion and metastasis. This mirrors the pathogen-driven metabolic hijacking described in macrophage polarization. Using COG133TFA to inhibit APOE in TAMs can induce a reduction in their transformation into M2 macrophages, leading to the release of CD8 + T cell inhibition. Combined blockade of PD-1 and TIGIT inhibitors can improve the efficiency of tumor regression [49]. This dual role of APOE in lipid metabolism and immune modulation underscores its significance in shaping the tumor immune landscape,

highlighting potential therapeutic avenues targeting APOE-mediated pathways to modulate macrophage polarization and enhance anti-tumor immunity. CD38 is a multifunctional transmembrane glycoprotein that plays a significant role in cancer biology through its enzymatic and signaling activities. As a nicotinamide adenine dinucleotide (NAD+) glycohydrolase and ADP-ribosyl cyclase, CD38 catalyzes the metabolism of NAD+ to produce calcium-mobilizing metabolites like cyclic ADP-ribose (cADPR) and adenosine diphosphate ribose (ADPR) [26]. These metabolites regulate intracellular calcium signaling, which influences cell proliferation, apoptosis, and immune responses. In cancer, CD38 is often overexpressed in malignancies such as multiple myeloma and chronic lymphocytic leukemia (CLL), where its high expression correlates with aggressive disease progression, enhanced cell survival, and resistance to therapy [26, 50]. Recent studies have also emphasized its role in glioma progression. CD38 is mainly expressed in M1 cells, but is less expressed in M2 cells, becoming a reliable surface marker for M1 macrophages, where CD38 deficiency in tumor-associated microglia/macrophages attenuates tumor growth, indicating its involvement in tumor-immune crosstalk [51]. This is also consistent with our results, as correlation analysis found that CD38 was positively correlated with M1 macrophages and negatively correlated with M2 cells. CD38-mediated NAD metabolism can also increase the cell's sensitivity to ferroptosis, and our in vitro experiments have also demonstrated that CD38 is a ferroptosis promoter, because overexpression of CD38 can induce an increase in ferroptosis-related indicators in PC-3 cells [51]. This suggests that CD38 is a promising target for synthetically inducing tumor cell death, but the specific mechanism still needs further exploration.

The analysis of tumor mutation burden and mutational landscape in PCa revealed significant differences between high-risk and low-risk groups, providing insights into the molecular heterogeneity driving disease progression. High-risk patients exhibited a substantially higher TMB ($p < 0.0001$), consistent with studies linking increased TMB to aggressive tumor behavior and poorer prognosis [52]. Notably, TP53 mutations were significantly more prevalent in the high-risk group (17% vs. 3%), aligning with its established role in promoting genomic instability and treatment resistance [53]. TP53 loss of function disrupts genomic stability, enhances tumor cell survival, and promotes resistance to standard therapies, which may explain the poorer prognosis in these patients [54]. This aligns with the increased prevalence of mutations in oncogenic pathways such as RTK-RAS, NOTCH, WNT, and Hippo, which are known to drive tumor proliferation, invasion, and metastasis. Additionally, TP53-mutated tumors may benefit from therapeutic strategies aimed at restoring p53 function or exploiting synthetic lethality, such as PARP inhibitors [54]. Further functional studies are necessary to delineate the precise roles of these mutations in prostate cancer and to develop effective personalized treatment strategies. In contrast, TTN was the most frequently mutated gene in the low-risk group, suggesting its potential role in less aggressive disease phenotypes. Pathway analysis further highlighted the molecular divergence between groups, with the RTK-RAS, NOTCH, WNT, and Hippo pathways more frequently altered in high-risk patients. These findings are consistent with prior studies implicating these pathways in PCa progression and metastasis [55, 56]. Interestingly, the model genes such as EZH2, APOE, and PTGS2 showed low CNV frequencies, indicating their stability and potential utility as reliable biomarkers. The higher mutation burden and pathway dysregulation in high-risk patients underscore the importance of genomic instability in driving aggressive disease, while the distinct mutational profiles of low-risk patients suggest a more stable genomic landscape. These findings align with emerging evidence that TMB and specific pathway alterations can stratify PCa patients for targeted therapies and immunotherapy [57]. Future studies should explore the functional impact of these mutations and their potential as therapeutic targets to improve outcomes in high-risk PCa patients.

The immune microenvironment plays a pivotal role in PCa progression and treatment response, as highlighted by our findings. The high-risk group exhibited significantly higher stromal, immune, and ESTIMATE scores, indicating a more active yet immunosuppressive tumor microenvironment (TME). This aligns with previous studies showing that increased immune infiltration, particularly of regulatory T cells (Tregs) and TAMs, is associated with poor prognosis and therapy resistance [58, 59]. Specifically, the elevated infiltration of CD8+T cells and M2 macrophages in the high-risk group suggests a paradoxical immune landscape where cytotoxic activity is counterbalanced by immunosuppressive mechanisms, such as Treg-mediated suppression and M2 macrophage-driven immune evasion [41, 60]. In addition, we also analyzed the expression differences of immune checkpoints between high-risk and low-risk groups and found that most immune checkpoints were elevated in the high-risk group, which helps to explain the paradoxical phenomenon that elevated immune checkpoints hinder the anti-tumor effect of CD8+T cells. In contrast, the low-risk group showed higher infiltration of plasma cells and neutrophils, which have been linked to better outcomes in some cancers due to their roles in antibody production and anti-tumor immunity [58, 61]. The strong association of APOE with M2 macrophages further underscores the role of lipid metabolism in shaping immunosuppressive TME, as APOE is known to promote M2 polarization and tumor progression [61]. Similarly, RIPK3's correlation with memory T cells highlights its potential role in modulating T cell exhaustion and immune surveillance [41]. The differential response to ICI therapy between high- and low-risk groups underscores the need for personalized treatment strategies. The low-risk group's higher response rate

(30% vs. 16%) and longer survival suggest that these patients may benefit more from immunotherapy, particularly ICIs targeting PD-1/PD-L1 or CTLA-4 [62]. Conversely, the high-risk group's resistance to ICI therapy, as indicated by higher TIDE and dysfunction scores, highlights the need for combination therapies that address immune evasion mechanisms, such as TAM-targeting agents or metabolic modulators [61]. It has been reported that modulating ferroptosis can significantly impact immunotherapy outcomes by altering the tumor microenvironment and enhancing immune responses. Strategies to induce ferroptosis include targeting lipid peroxidation with small-molecule inducers (e.g., erastin, RSL3), inhibiting GPX4, or modulating iron metabolism via transferrin receptor upregulation [63]. Ferroptosis can enhance immunotherapy efficacy by increasing tumor antigen release, promoting dendritic cell activation, and improving T-cell infiltration. Additionally, ferroptotic tumor cells release damage-associated molecular patterns (DAMPs), which enhance anti-tumor immunity [64]. However, some tumors develop resistance by upregulating antioxidant defenses or ferroptosis-suppressing pathways. Combining ferroptosis inducers with immune checkpoint inhibitors could overcome resistance, enhancing tumor immunogenicity and response rates. Future research should focus on identifying biomarkers to predict ferroptosis sensitivity and optimizing combination strategies to maximize therapeutic benefits while minimizing toxicity. Additionally, our model also helps predict sensitivity to chemotherapy drugs, such as Erlotinib and Picolinic acid, which may benefit low-risk patients, but their side effects also need to be noted. Erlotinib, an EGFR inhibitor targeting the RTK-RAS pathway, has shown efficacy in cancers with EGFR/RAS dysregulation. However, in PCa, its clinical utility remains underexplored. Common side effects include rash, diarrhea, and fatigue, while rare but severe toxicities include interstitial lung disease. Early-phase trials in PCa (e.g., NCT00443235) reported limited efficacy, possibly due to compensatory signaling or low EGFR dependence in unselected cohorts [65, 66]. Picolinic acid, a metal ion chelator, exhibits preclinical anti-tumor activity by modulating NOTCH/WNT pathways and immune responses [67]. While well-tolerated in animal studies, its human safety profile remains unvalidated, and no PCa-specific clinical trials are registered. Both agents require biomarker-driven trials to identify responsive subsets. For instance, combining Erlotinib with RAS/MAPK pathway inhibitors or pairing Picolinic acid with immunotherapy may overcome resistance.

Despite the promising findings of our study, several limitations should be acknowledged. First, our prognostic model was developed and validated using publicly available datasets, which may introduce selection bias and limit its generalizability to broader patient populations. Prospective, multi-center studies are needed to further validate its clinical applicability. Second, although our analysis suggests significant differences in immune infiltration and immunotherapy response between risk groups, these findings are based on computational predictions rather than direct clinical validation. Experimental studies, including functional assays and patient-derived models, are necessary to confirm these associations. Additionally, while our drug sensitivity analysis identified potential therapeutic agents, in vitro and in vivo experiments are required to verify their efficacy in high- and low-risk patients. Finally, the complexity of tumor heterogeneity and microenvironmental interactions may not be fully captured by bulk transcriptomic data, highlighting the need for single-cell and spatial transcriptomic studies to provide deeper insights into the molecular mechanisms driving disease progression and treatment response.

In conclusion, our study highlights the critical role of the immune microenvironment in PCa risk stratification and treatment response. By elucidating the molecular and cellular mechanisms underlying these differences, we provide a foundation for developing precision immunotherapy strategies tailored to individual patient risk profiles. Future research should focus on validating these findings in larger, multi-center cohorts and exploring therapeutic strategies to reprogram the immunosuppressive TME in high-risk PCa. For instance, targeting APOE-mediated lipid metabolism or RIPK3-regulated T-cell exhaustion could enhance ICI efficacy. Additionally, integrating single-cell and spatial transcriptomics could provide deeper insights into the spatial organization of immune cells and their interactions within the TME.

Acknowledgements Thanks a lot to the contributors to the public datasets, raw data can be obtained by following the link provided.

Author contributions Zhenwei Wang wrote the paper, Zhihong Dai prepared Figs. 1, 2, 3, 4, and 5, Yuren Gao prepared Figs. 6, 7, Zongxiang Zhao collected data and prepared Figs. 8, 9, Zhen Li collected data and cultured cells, Liang Wang, and Xiang Gao revised and polished the language, Qiuqiu Qiu conducted in vitro experiments and prepared Fig. 10. Xiaofu Qiu revised the paper, Zhiyu Liu Design and organized the study. All authors reviewed the manuscript.

Funding The Scientific Research Project of the Ministry of Education of Liaoning Province (LJKZZ20220100); The Interdisciplinary Research Cooperation Project Team Funding of Dalian Medical University Planning and Research category (focusing on planning for recreation) (JCHZ2023001); The United Foundation for Dalian Institute of Chemical Physics. Chinese Academy of Sciences and the Second Hospital of Dalian Medical University (DMU-2 & DICP UN202304); Science and Technology Planning Project of Guangzhou City, Guangdong, China (Grant No. 202201020582); "1 + X" program for Clinical Competency enhancement–Clinical Technical Level Improvement Project, The Second Hospital of Dalian Medical University (2022LCJSGC16).

Data availability The datasets generated during and/or analyzed during the current study are available from the corresponding author on reasonable request.

Declarations

Ethics approval and consent to participate Not available, for the study used only public database samples and did not involve collecting human or animal specimens for experiments.

Competing interests The authors declare no competing interests.

References

1. Bray F, Laversanne M, Sung H, Ferlay J, Siegel RL, Soerjomataram I, Jemal A. Global cancer statistics 2022: GLOBOCAN estimates of incidence and mortality worldwide for 36 cancers in 185 countries. CA Cancer J Clin. 2024;74:229–63. https://doi.org/10.3322/caac.21834.
2. Currie E, Schulze A, Zechner R, Walther TC, Farese RV. Cellular fatty acid metabolism and cancer. Cell Metab. 2013;18:153–61. https://doi.org/10.1016/j.cmet.2013.05.017.
3. Liu Y, Sun Y, Guo Y, Shi X, Chen X, Feng W, Wu LL, et al. An overview: the diversified role of mitochondria in cancer metabolism. Int J Biol Sci. 2023;19:897–915. https://doi.org/10.7150/ijbs.81609.
4. Luo Y, Wang H, Liu B, Wei J. Fatty acid metabolism and cancer immunotherapy. Curr Oncol Rep. 2022;24:659–70. https://doi.org/10.1007/s11912-022-01223-1.
5. Koundouros N, Poulogiannis G. Reprogramming of fatty acid metabolism in cancer. Br J Cancer. 2020;122:4–22. https://doi.org/10.1038/s41416-019-0650-z.
6. Xu L, Zhang Y, Lin Z, Deng X, Ren X, Huang M, Li S, et al. FASN-mediated fatty acid biosynthesis remodels immune environment in Clonorchis sinensis infection-related intrahepatic cholangiocarcinoma. J Hepatol. 2024;81:265–77. https://doi.org/10.1016/j.jhep.2024.03.016.
7. Ito H, Nakamae I, Kato J-Y, Yoneda-Kato N. Stabilization of fatty acid synthesis enzyme acetyl-CoA carboxylase 1 suppresses acute myeloid leukemia development. J Clin Investig. 2021. https://doi.org/10.1172/JCI141529.
8. Lien EC, Westermark AM, Zhang Y, Yuan C, Li Z, Lau AN, Sapp KM, Wolpin BM, Heiden MGV. Low glycaemic diets alter lipid metabolism to influence tumour growth. Nature. 2021;599:302–7. https://doi.org/10.1038/s41586-021-04049-2.
9. Ma Y, Zhang X, Alsaidan OA, Yang X, Sulejmani E, Zha J, Beharry Z, et al. Long-chain Acyl-CoA synthetase 4-mediated fatty acid metabolism sustains androgen receptor pathway-independent prostate cancer. Mol Cancer Res MCR. 2021;19:124–35. https://doi.org/10.1158/1541-7786.MCR-20-0379.
10. Xu H, Chen Y, Meng Gu, Liu C, Chen Qi, Zhan M, Wang Z. Fatty acid metabolism reprogramming in advanced prostate cancer. Metabolites. 2021. https://doi.org/10.3390/metabo11110765.
11. Guo Y, Zheng Z, Mao S, Yang F, Wang R, Wang H, Liu Ji, et al. Metabolic-associated signature and hub genes associated with immune microenvironment and prognosis in bladder cancer. Mol Carcinog. 2023;62:185–99. https://doi.org/10.1002/mc.23475.
12. Tong X, Tang R, Xiao M, Jin Xu, Wang W, Zhang Bo, Liu J, Xianjun Yu, Shi Si. Targeting cell death pathways for cancer therapy: recent developments in necroptosis, pyroptosis, ferroptosis, and cuproptosis research. J Hematol Oncol. 2022;15:174. https://doi.org/10.1186/s13045-022-01392-3.
13. Shrestha RK, Nassar ZD, Hanson AR, Iggo R, Townley SL, Dehairs J, Mah CY, et al. ACSM1 and ACSM3 regulate fatty acid metabolism to support prostate cancer growth and constrain ferroptosis. Can Res. 2024;84:2313–32. https://doi.org/10.1158/0008-5472.CAN-23-1489.
14. Ding K, Liu C, Li Li, Yang M, Jiang Na, Luo S, Sun L. Acyl-CoA synthase ACSL4: an essential target in ferroptosis and fatty acid metabolism. Chin Med J. 2023;136:2521–37. https://doi.org/10.1097/CM9.0000000000002533.
15. Liao P, Wang W, Wang W, Kryczek I, Li X, Bian Y, Sell A, et al. CD8(+) T cells and fatty acids orchestrate tumor ferroptosis and immunity via ACSL4. Cancer Cell. 2022;40:365-378.e6. https://doi.org/10.1016/j.ccell.2022.02.003.
16. Sen U, Coleman C, Sen T. Stearoyl coenzyme A desaturase-1: multitasker in cancer, metabolism, and ferroptosis. Trends Cancer. 2023;9:480–9. https://doi.org/10.1016/j.trecan.2023.03.003.
17. Hao J-W, Wang J, Guo H, Zhao Y-Y, Sun H-H, Li Y-F, Lai X-Y, et al. CD36 facilitates fatty acid uptake by dynamic palmitoylation-regulated endocytosis. Nat Commun. 2020;11:4765. https://doi.org/10.1038/s41467-020-18565-8.
18. Lee J-Y, Nam M, Son HY, Hyun K, Jang SY, Kim JW, Kim MW, et al. Polyunsaturated fatty acid biosynthesis pathway determines ferroptosis sensitivity in gastric cancer. Proc Natl Acad Sci USA. 2020;117:32433–42. https://doi.org/10.1073/pnas.2006828117.
19. Huang Xi, Sun Y, Song J, Huang Y, Shi H, Qian A, Cao Y, Zhou Y, Wang Q. Prognostic value of fatty acid metabolism-related genes in colorectal cancer and their potential implications for immunotherapy. Front Immunol. 2023;14:1301452. https://doi.org/10.3389/fimmu.2023.1301452.

20. Tang Y, Tian W, Xie J, Zou Y, Wang Z, Li N, Zeng Y, et al. Prognosis and dissection of immunosuppressive microenvironment in breast cancer based on fatty acid metabolism-related signature. Front Immunol. 2022;13:843515. https://doi.org/10.3389/fimmu.2022.843515.
21. Yang C, Zhang H, Chen M, Wang S, Qian R, Zhang L, Huang X, et al. A survey of optimal strategy for signature-based drug repositioning and an application to liver cancer. eLife. 2022;11:e71880. https://doi.org/10.7554/eLife.71880.
22. Martínez-Jiménez F, Muiños F, Sentís I, Deu-Pons J, Reyes-Salazar I, Arnedo-Pac C, Mularoni L, et al. A compendium of mutational cancer driver genes. Nat Rev Cancer. 2020;20:555–72. https://doi.org/10.1038/s41568-020-0290-x.
23. Moore AR, Rosenberg SC, McCormick F, Malek S. RAS-targeted therapies: is the undruggable drugged? *Nature reviews*. Drug Discov. 2020;19:533–52. https://doi.org/10.1038/s41573-020-0068-6.
24. Waarts MR, Stonestrom AJ, Park YC, Levine RL. Targeting mutations in cancer. J Clin Investig. 2022. https://doi.org/10.1172/JCI154943.
25. Rao A, Barkley D, França GS, Yanai I. Exploring tissue architecture using spatial transcriptomics. Nature. 2021;596:211–20. https://doi.org/10.1038/s41586-021-03634-9.
26. Chini EN, Chini CCS, Netto JME, de Oliveira GC, van Schooten W. The pharmacology of CD38/NADase: an emerging target in cancer and diseases of aging. Trends Pharmacol Sci. 2018;39:424–36. https://doi.org/10.1016/j.tips.2018.02.001.
27. Li Y, Yang R, Chen L, Sufang Wu. CD38 as an immunomodulator in cancer. Future Oncol. 2020;16:2853–61. https://doi.org/10.2217/fon-2020-0401.
28. Chmielewski JP, Bowlby SC, Wheeler FB, Shi L, Sui G, Davis AL, Howard TD, et al. CD38 inhibits prostate cancer metabolism and proliferation by reducing cellular NAD(+) pools. Mol Cancer Res MCR. 2018;16:1687–700. https://doi.org/10.1158/1541-7786.MCR-17-0526.
29. Kanayama M, Luo J. CD38-induced apoptosis and mitochondrial damage is restored by nicotinamide in prostate cancer. Front Mol Biosci. 2022;9:890402. https://doi.org/10.3389/fmolb.2022.890402.
30. Klein EA, Cooperberg MR, Magi-Galluzzi C, Simko JP, Falzarano SM, Maddala T, Chan JM, et al. A 17-gene assay to predict prostate cancer aggressiveness in the context of Gleason grade heterogeneity, tumor multifocality, and biopsy undersampling. Eur Urol. 2014;66:550–60. https://doi.org/10.1016/j.eururo.2014.05.004.
31. Ross AE, Johnson MH, Yousefi K, Davicioni E, Netto GJ, Marchionni L, Fedor HL, et al. Tissue-based genomics augments post-prostatectomy risk stratification in a natural history cohort of intermediate- and high-risk men. Eur Urol. 2016;69:157–65. https://doi.org/10.1016/j.eururo.2015.05.042.
32. Erho N, Crisan A, Vergara IA, Mitra AP, Ghadessi M, Buerki C, Bergstralh EJ, et al. Discovery and validation of a prostate cancer genomic classifier that predicts early metastasis following radical prostatectomy. PLoS ONE. 2013;8:e66855. https://doi.org/10.1371/journal.pone.0066855.
33. Tibshirani R. The lasso method for variable selection in the Cox model. Stat Med. 1997;16:385–95. https://doi.org/10.1002/(sici)1097-0258(19970228)16:4%3c385::aid-sim380%3e3.0.co;2-3.
34. Cooperberg MR, Hilton JF, Carroll PR. The CAPRA-S score: a straightforward tool for improved prediction of outcomes after radical prostatectomy. Cancer. 2011;117:5039–46. https://doi.org/10.1002/cncr.26169.
35. Parker JS, Mullins M, Cheang MCU, Leung S, Voduc D, Vickery T, Davies S, et al. Supervised risk predictor of breast cancer based on intrinsic subtypes. J Clin Oncol. 2023;41:4192–9. https://doi.org/10.1200/JCO.22.02511.
36. Zhou Y, Zhou H, Hua L, Hou C, Jia Q, Chen J, Zhang S, Wang Y, He S, Jia E. Verification of ferroptosis and pyroptosis and identification of PTGS2 as the hub gene in human coronary artery atherosclerosis. Free Radical Biol Med. 2021;171:55–68. https://doi.org/10.1016/j.freeradbiomed.2021.05.009.
37. Giunchi F, Fiorentino M, Loda M. The metabolic landscape of prostate cancer. Eur Urol Oncol. 2019;2:28–36. https://doi.org/10.1016/j.euo.2018.06.010.
38. Kulminski AM, Jain-Washburn E, Nazarian A, Wilkins HM, Veatch O, Swerdlow RH, Honea RoA. Association of APOE alleles and polygenic profiles comprising APOE-TOMM40-APOC1 variants with Alzheimer's disease neuroimaging markers. Alzheimer's & Dementia. 2024. https://doi.org/10.1002/alz.14445.
39. Spranger S, Sivan A, Corrales L, Gajewski TF. Tumor and host factors controlling antitumor immunity and efficacy of cancer immunotherapy. Adv Immunol. 2016;130:75–93. https://doi.org/10.1016/bs.ai.2015.12.003.
40. Massie CE, Lynch A, Ramos-Montoya A, Boren J, Stark R, Fazli L, Warren A, et al. The androgen receptor fuels prostate cancer by regulating central metabolism and biosynthesis. EMBO J. 2011;30:2719–33. https://doi.org/10.1038/emboj.2011.158.
41. Hirz T, Mei S, Sarkar H, Kfoury Y, Shulin Wu, Verhoeven BM, Subtelny AO, et al. Dissecting the immune suppressive human prostate tumor microenvironment via integrated single-cell and spatial transcriptomic analyses. Nat Commun. 2023;14:663. https://doi.org/10.1038/s41467-023-36325-2.
42. Feng D-C, Zhu W-Z, Wang J, Deng-Xiong Li Xu, Shi QX, You J, et al. The implications of single-cell RNA-seq analysis in prostate cancer: unraveling tumor heterogeneity, therapeutic implications and pathways towards personalized therapy. Mil Med Res. 2024;11:21. https://doi.org/10.1186/s40779-024-00526-7.
43. Lyu A, Fan Z, Clark M, Lea A, Luong D, Setayesh A, Starzinski A, et al. Evolution of myeloid-mediated immunotherapy resistance in prostate cancer. Nature. 2025;637:1207–17. https://doi.org/10.1038/s41586-024-08290-3.
44. Kiviaho A, Eerola SK, Kallio HML, Andersen MK, Hoikka M, Tiihonen AM, Salonen I, et al. Single cell and spatial transcriptomics highlight the interaction of club-like cells with immunosuppressive myeloid cells in prostate cancer. Nat Commun. 2024;15:9949. https://doi.org/10.1038/s41467-024-54364-1.
45. Bian X, Wang W, Abudurexiti M, Zhang X, Ma W, Shi G, Du L, et al. Integration analysis of single-cell multi-omics reveals prostate cancer heterogeneity. Adv Sci. 2024;11:e2305724. https://doi.org/10.1002/advs.202305724.
46. Bancaro N, Calì B, Troiani M, Elia AR, Arzola RA, Attanasio G, Lai P, et al. Apolipoprotein E induces pathogenic senescent-like myeloid cells in prostate cancer. Cancer Cell. 2023;41:602-619.e11. https://doi.org/10.1016/j.ccell.2023.02.004.
47. Wong HY, Sheng Q, Hesterberg AB, Croessmann S, Rios BL, Giri K, Jackson J, et al. Single cell analysis of cribriform prostate cancer reveals cell intrinsic and tumor microenvironmental pathways of aggressive disease. Nat Commun. 2022;13:6036. https://doi.org/10.1038/s41467-022-33780-1.

48. Kemp SB, Carpenter ES, Steele NG, Donahue KL, Nwosu ZC, Pacheco A, Velez-Delgado A, et al. Apolipoprotein E promotes immune suppression in pancreatic cancer through NF-κB-mediated production of CXCL1. Can Res. 2021;81:4305–18. https://doi.org/10.1158/0008-5472.CAN-20-3929.
49. Hui B, Chen Lu, Li H, Hao X, Liu H, Zhuo D, Wang Q, et al. Inhibition of APOE potentiates immune checkpoint therapy for cancer. Int J Biol Sci. 2022;18:5230–40. https://doi.org/10.7150/ijbs.70117.
50. Gozzetti A, Ciofini S, Simoncelli M, Santoni A, Pacelli P, Raspadori D, Bocchia M. Anti CD38 monoclonal antibodies for multiple myeloma treatment. Hum Vaccin Immunother. 2022;18:2052658. https://doi.org/10.1080/21645515.2022.2052658.
51. Levy A, Blacher E, Vaknine H, Lund FE, Stein R, Mayo L. CD38 deficiency in the tumor microenvironment attenuates glioma progression and modulates features of tumor-associated microglia/macrophages. Neuro Oncol. 2012;14:1037–49. https://doi.org/10.1093/neuonc/nos121.
52. Chalmers ZR, Connelly CF, Fabrizio D, Gay L, Ali SM, Ennis R, Schrock A, et al. Analysis of 100,000 human cancer genomes reveals the landscape of tumor mutational burden. Genome Med. 2017;9:34. https://doi.org/10.1186/s13073-017-0424-2.
53. Kandoth C, McLellan MD, Vandin F, Ye K, Niu B, Charles Lu, Xie M, et al. Mutational landscape and significance across 12 major cancer types. Nature. 2013;502:333–9. https://doi.org/10.1038/nature12634.
54. Marei HE, Althani A, Afifi N, Hasan A, Caceci T, Pozzoli G, Morrione A, Giordano A, Cenciarelli C. p53 signaling in cancer progression and therapy. Cancer Cell Int. 2021;21:703. https://doi.org/10.1186/s12935-021-02396-8.
55. Abida W, Cyrta J, Heller G, Prandi D, Armenia J, Coleman I, Cieslik M, et al. Genomic correlates of clinical outcome in advanced prostate cancer. Proc Natl Acad Sci USA. 2019;116:11428–36. https://doi.org/10.1073/pnas.1902651116.
56. Robinson D, Van Allen EM, Yi-Mi Wu, Schultz N, Lonigro RJ, Mosquera J-M, Montgomery B, et al. Integrative clinical genomics of advanced prostate cancer. Cell. 2015;161:1215–28. https://doi.org/10.1016/j.cell.2015.05.001.
57. Alexandrov LB, Kim J, Haradhvala NJ, Huang MN, Ng AWT, Yang Wu, Boot A, et al. The repertoire of mutational signatures in human cancer. Nature. 2020;578:94–101. https://doi.org/10.1038/s41586-020-1943-3.
58. Chen L, Yu-Xin Xu, Wang Y-S, Ren Y-Y, Xue-Man Dong PuWu, Xie T, Zhang Qi, Zhou J-L. Prostate cancer microenvironment: multidimensional regulation of immune cells, vascular system, stromal cells, and microbiota. Mol Cancer. 2024;23:229. https://doi.org/10.1186/s12943-024-02137-1.
59. Novysedlak R, Guney M, Khouri MA, Bartolini R, Foley LK, Benesova I, Ozaniak A, et al. The immune microenvironment in prostate cancer: a comprehensive review. Oncology. 2024. https://doi.org/10.1159/000541881.
60. Anton A, Hutchinson R, Hovens CM, Christie M, Ryan A, Gibbs P, Costello A, et al. An immune suppressive tumor microenvironment in primary prostate cancer promotes tumor immune escape. PLoS ONE. 2024;19:e0301943. https://doi.org/10.1371/journal.pone.0301943.
61. Yang B, Jiang Y, Yang J, Zhou W, Yang T, Zhang R, Jinming Xu, Guo H. Characterization of metabolism-associated molecular patterns in prostate cancer. BMC Urol. 2023;23:104. https://doi.org/10.1186/s12894-023-01275-w.
62. Tsaur I, Brandt MP, Juengel E, Manceau C, Ploussard G. Immunotherapy in prostate cancer: new horizon of hurdles and hopes. World J Urol. 2021;39:1387–403. https://doi.org/10.1007/s00345-020-03497-1.
63. Li J, Liu J, Zhou Z, Wu R, Chen X, Yu C, Stockwell B, Kroemer G, Kang R, Tang D. Tumor-specific GPX4 degradation enhances ferroptosis-initiated antitumor immune response in mouse models of pancreatic cancer. Sci Transl Med. 2023;15:3049. https://doi.org/10.1126/scitranslmed.adg3049.
64. Lin Z, Zou S, Wen K. The crosstalk of CD8+ T cells and ferroptosis in cancer. Front Immunol. 2023;14:1255443. https://doi.org/10.3389/fimmu.2023.1255443.
65. Nabhan C, Lestingi TM, Galvez A, Tolzien K, Kelby SK, Tsarwhas D, Newman S, Bitran JD. Erlotinib has moderate single-agent activity in chemotherapy-naïve castration-resistant prostate cancer: final results of a phase II trial. Urology. 2009;74:665–71. https://doi.org/10.1016/j.urology.2009.05.016.
66. Gross M, Higano C, Pantuck A, Castellanos O, Green E, Nguyen K, Agus DB. A phase II trial of docetaxel and erlotinib as first-line therapy for elderly patients with androgen-independent prostate cancer. BMC Cancer. 2007;7:142. https://doi.org/10.1186/1471-2407-7-142.
67. Matlou ML, Malan FP, Nkadimeng S, McGaw L, Tembu VJ, Manicum A-L. Exploring the in vitro anticancer activities of Re(I) picolinic acid and its fluorinated complex derivatives on lung cancer cells: a structural study. J Biol Inorg Chem. 2023;28:29–41. https://doi.org/10.1007/s00775-022-01971-2.